

K. Shah

Department of Mechanical and Aerospace Engineering,
The University of Texas at Arlington,
Arlington, TX 76019

N. Balsara

Department of Chemical and Biomolecular Engineering,
University of California at Berkeley,
Berkeley, CA 94720

S. Banerjee

School of Mechanical and Materials Engineering,
Washington State University,
Pullman, WA 99164

M. Chintapalli

Department of Chemical and Biomolecular Engineering,
University of California at Berkeley,
Berkeley, CA 94720

A. P. Cocco

Department of Mechanical Engineering,
University of Connecticut,
Storrs, CT 06269

W. K. S. Chiu

Department of Mechanical Engineering,
University of Connecticut,
Storrs, CT 06269

I. Lahiri

Department of Metallurgical and Materials Engineering,
Indian Institute of Technology Roorkee,
Roorkee 247667, India

S. Martha

Department of Chemistry,
Indian Institute of Technology Hyderabad,
Hyderabad 502285, India

A. Mistry

Department of Mechanical Engineering,
Texas A&M University,
College Station, TX 77843

P. P. Mukherjee

Department of Mechanical Engineering,
Texas A&M University,
College Station, TX 77843

V. Ramadesigan

Department of Energy Science and Engineering,
Indian Institute of Technology Bombay,
Mumbai 400076, India

C. S. Sharma

Department of Chemical Engineering,
Indian Institute of Technology Hyderabad,
Hyderabad 502285, India

V. R. Subramanian

Department of Chemical Engineering,
University of Washington,
Seattle, WA 98105

S. Mitra

Department of Energy Science and Engineering,
Indian Institute of Technology Bombay,
Mumbai 400076, India

A. Jain¹

Department of Mechanical and Aerospace Engineering,
The University of Texas at Arlington,
Arlington, TX 76019
e-mail: jaina@uta.edu

State of the Art and Future Research Needs for Multiscale Analysis of Li-Ion Cells

The performance, safety, and reliability of Li-ion batteries are determined by a complex set of multiphysics, multiscale phenomena that must be holistically studied and optimized. This paper provides a summary of the state of the art in a variety of research fields related to Li-ion battery materials, processes, and systems. The material presented here is based on a series of discussions at a recently concluded bilateral workshop in which researchers and students from India and the U.S. participated. It is expected that this summary will help understand the complex nature of Li-ion batteries and help highlight the critical directions for future research. [DOI: 10.1115/1.4036456]

¹Corresponding author.

Manuscript received February 6, 2017; final manuscript received March 24, 2017; published online May 16, 2017. Assoc. Editor: Kevin Huang.

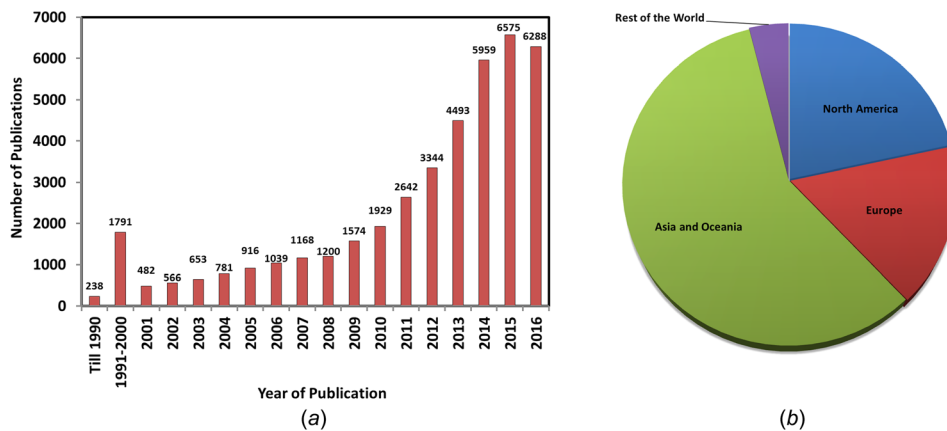


Fig. 1 (a) Yearwise publication trend and (b) demographic distribution of Li-ion battery research

1 Introduction

Li-ion batteries are a technologically important class of electrochemical energy conversion and storage devices that offer very large energy density and power output. The performance and safety of Li-ion batteries are based upon a remarkably complicated set of highly coupled transport processes that occur over multiple lengthscales. As a result, a systematic analysis of these phenomena and their coupling with each other as well as measurement of transport parameters and experimental validation of theoretical/numerical models are very important not only for ensuring high performance and safety of present Li-ion cells but also for guiding materials choices and cell design for future devices. Due to the technologically important nature of Li-ion cells, as well as the scientific richness of underlying physical processes, a significant amount of research has been carried out worldwide. Figure 1(a) shows a tremendous increase in the number of journal papers related to Li-ion batteries published since 1990, based on the data from the website.² Figure 1(b) shows the geographical breakdown of these papers, indicating the largest fraction of contributions from Asian and Oceanic countries.³

Research progress is often reported in a wide variety of professional society meetings. In an attempt to bring together experts from a variety of different technical backgrounds related to Li-ion batteries, the Indo-US Workshop on Recent Advances in Multiphysics Analysis of Li-Ion Cells was organized in Mumbai, India on June 17–19, 2016. This workshop was co-organized by the University of Texas at Arlington, Arlington, TX and Indian Institute of Technology, Bombay (IITB), Mumbai, India. A total of ten institutions from the U.S. and ten institutions from India participated in technical seminars and discussions during the workshop. The range of technical expertise represented in the workshop included materials scientists, chemical engineers, mechanical engineers, physicists, chemists, and others with multidisciplinary affiliations. There was a strong student participation from both countries.

This review paper summarizes the wide variety of technical discussions during the workshop through brief discussions of recent progress and future research needs in several technical directions relevant to the analysis and optimization of Li-ion batteries. These topics include future materials, modeling techniques, visualization tools, etc.

2 Thermodynamics, Grain Structure, and Ion Transport in Block Copolymer/Salt Mixtures

Phase-separated block copolymer/salt mixtures in which one phase is mechanically rigid and the other phase solvates and

transports ions from the salt are promising materials for a wide range of applications including high-energy density lithium metal battery electrolytes, fuel cells, and photoelectrochemical fuel production. Ion transport in these materials is strongly dependent on the thermodynamics of phase separation and the grain structure of the block copolymer morphology, neither of which are well-understood in salt-containing block copolymers.

A model material for lithium battery electrolytes is lamellar polystyrene-*block*-poly(ethylene oxide) mixed with lithium bis(trifluoromethanesulfonyl) imide salt (SEO/LiTFSI). The polystyrene (PS) block is mechanically rigid and the poly(ethylene oxide) (PEO) block solvates and transports LiTFSI salt. We report on the progress toward understanding the relationships between ion transport, thermodynamics, and grain structure in this system.

In electrolytes consisting of homopolymer/salt mixtures, the relationship between ionic conductivity and salt concentration exhibits a simple maximum. In PEO/LiTFSI, the maximum occurs at a salt concentration around $r=0.1$, where r is the ratio of salt molecules to ethylene oxide repeat units. Most literature on SEO/LiTFSI has therefore focused on low salt concentrations around $r=0.1$ [1]. We recently reported on characterization of grain size and conductivity in SEO/LiTFSI over a wider range of salt concentrations, up to $r=0.4$. [2]. Surprisingly, in SEO/LiTFSI, the relationship between ionic conductivity and salt concentration exhibits two maxima (Fig. 2), and the global maximum in ionic

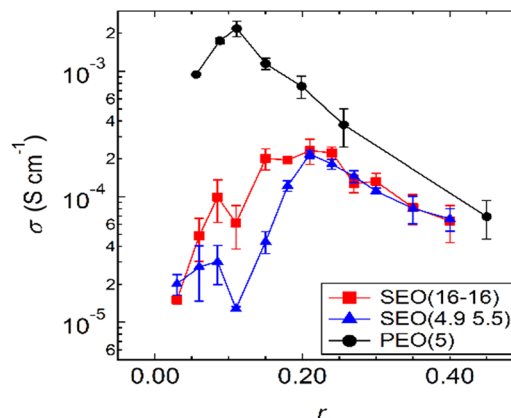


Fig. 2 Relationship between ionic conductivity, σ , and salt concentration, r , in SEO/LiTFSI and PEO/LiTFSI mixtures at 90 °C. The molecular weights of the polystyrene and poly(ethylene oxide) blocks are given in kilogram mole in parentheses. Ionic conductivity in PEO exhibits a simple maximum, whereas ionic conductivity in SEO has two local maxima.

²www.scopus.com

³Source: www.scopus.com

conductivity occurs at $r=0.21$, double the concentration that maximizes ionic conductivity in PEO.

Using small angle X-ray scattering (SAXS), we determined that the grain size decreases as a function of salt concentration (Fig. 3), and that this decrease correlates with an increase in ionic conductivity. We discovered that the dependence of ionic conductivity on salt concentration is fundamentally different in block copolymer electrolytes than in homopolymer electrolytes due to salt-induced changes in grain structure. Salt has complex effects on block copolymer grain structure and ion transport.

Salt-containing block copolymers often have inaccessible order-to-disorder transitions (ODT) due to the high Flory–Huggins interaction parameters in these systems. However, most studies on grain structure in block copolymers focus on systems that can be disordered. We explore grain evolution in an SEO/LiTFSI mixture that remains lamellar at all the temperatures. Two techniques commonly used to study grain structure in block copolymers are SAXS and depolarized light scattering (DPLS) [3]. DPLS has not previously been used to characterize grain evolution in fully ordered block copolymers. We published a study comparing SAXS and DPLS observations of grain evolution during the annealing of a fully ordered SEO/LiTFSI block copolymer. In SAXS, grains up to around 80 nm can be observed, and the upper bound is set by the minimum spot size that can be achieved in the X-ray beam [4]. In DPLS, grains above approximately 500 nm can be observed, and the lower bound is set by the wavelength of visible light used to probe the sample. Combining techniques allows changes in grain size to be monitored over a broad range of length scales.

The changes in grain size with annealing time observed by SAXS are qualitatively different from changes in grain size observed with DPLS (Fig. 4). In the SAXS regime, grain size increases with annealing temperature, and in the DPLS regime, grain size decreases with temperature. To explain this surprising observation, we propose that two populations of grains exist in the sample: a small population under 80 nm that grows with annealing (observed by SAXS), and a larger population above 500 nm that remains static or grows slowly with annealing (observed by DPLS). As more grains from the small population grow and enter the large population regime, the average size in the large population regime is observed to decrease. As further evidence that the size regime of the experimental technique impacts the observed grain size, DPLS was performed using two different wavelengths for the light sources, 640 nm and one at 473 nm. The average grain

size observed using the 640 nm light source is larger than the average grain size observed using the 473 nm light source (Fig. 5), as smaller grains can be observed with the 473 nm source. By combining data from multiple techniques, a more complete picture of grain structure in a block copolymer electrolyte was developed.

3 Carbon Xerogels as Anode for Lithium-Ion Batteries: Present Status and Future Perspectives

Since their introduction by Pekala and coworkers in 1989 [5], resorcinol–formaldehyde (RF)-based organic gels have received a considerable attention in literature to synthesize a wide variety of materials: highly porous aerogels to moderately porous cryogels to nearly nonporous xerogels, as per the drying pattern [6]. The same has been pyrolyzed at high temperature (e.g., 900 °C) in the inert atmosphere to yield correspondingly carbon gels. Owing to their high porosity and specific surface area, RF-derived carbon aerogels and cryogels have been used for many applications including as thermal insulator and electrode materials in electrochemical double-layer supercapacitors [6]. On the other hand, RF-derived carbon xerogels have not been explored to their full potential until very recently, primarily due to their nonporous characteristics. In the last decade or so, there are many studies which suggest that it is possible to fine tune the structural properties of RF-derived carbon xerogel including making them porous simply by altering the RF sol chemistry and controlling the synthesis conditions [7–15]. Further, it has been demonstrated that RF-derived carbon xerogel can be intercalated reversibly with lithium ions [16,17], this unwraps the tremendous potential of RF-derived carbon xerogels as anode materials for lithium-ion batteries and other similar energy storage devices. We here present the current status of this material for its application as anode and pitch in for its further perspectives to explore its full potential.

RF xerogels are formed by the polycondensation of resorcinol with formaldehyde in alkaline conditions followed by subcritical drying. There are few reports in which acidic catalysts are also used in organic solvent media [6]. In subcritical drying, solvent is evaporated by air oven drying at ambient pressure that changes the solvent surface tension drastically, thereby inducing large capillary forces at the liquid–vapor interfaces [18]. This phenomenon leads to shrinkage followed by collapse of porous structure yielding dense RF xerogel structures. There are now few reports available in literature on RF xerogels with moderate porosity also by

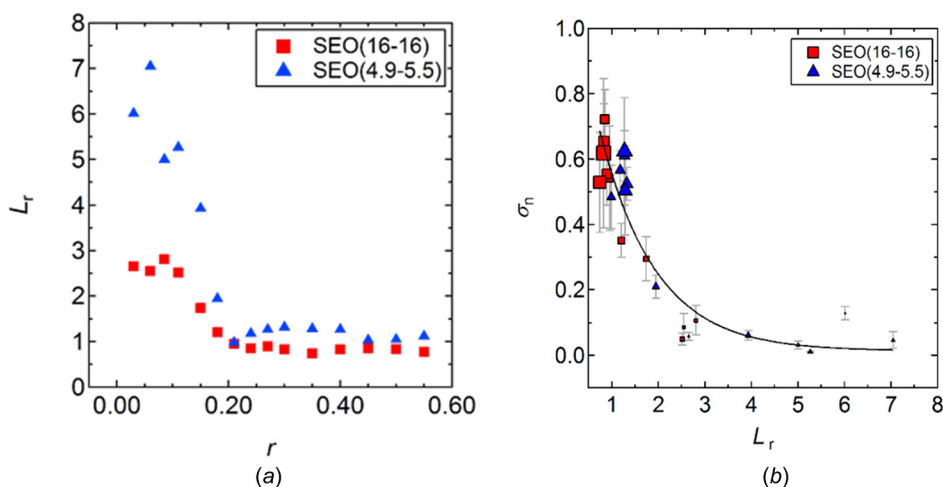


Fig. 3 (a) Grain size, L_r , expressed as a number of lamellae per grain, is plotted as a function of salt concentration, r . Grain size decreases as salt concentration increases, in SEO/LiTFSI of two different molecular weights. (b) Conductivity of SEO/LiTFSI normalized by the conductivity and volume fraction of PEO/LiTFSI, σ_n , is plotted as a function of L_r . The marker shows the concomitant changes in r . Larger markers represent higher values of r . Normalized conductivity decreases as grain size increases.

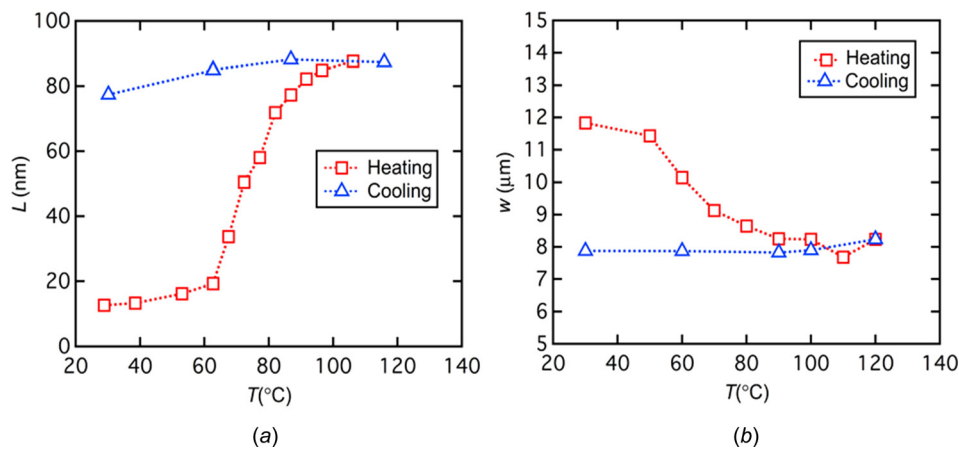


Fig. 4 (a) Grain size measured by small angle X-ray scattering, L , is plotted as a function of temperature during the anneal. (b) Grain size measured by DPLS, w , is plotted as a function of temperature during the anneal. The data in (a) show an increase in grain size upon heating, and the data in (b) show a decrease in grain size.

either tailoring the pH conditions of the RF sol [7,9] or by surface activation [19,20].

In the last decade or so, to explore the use of RF xerogels for different applications, there were many studies to synthesize a wide variety of morphologies that include hollow and solid microspheres, nanospheres, hierarchical microstructures, bowl-like, capsules, and high external surface area folded, needlelike, and fractal-like structures [7,8,10,11,13,14,21]. Most of these studies were based on modifying the RF sol precursor chemistry by tuning the experimental parameters, such as catalyst concentration, pH, temperature either during the sol-gel polycondensation or varying the surfactant concentration, type of surfactant and stirring conditions used in the next step, inverse emulsion polymerization. RF sol has also been electrosprayed to produce sub-100 nm xerogel particles [22] while it is mixed with other polymer carrier to generate ultrathin electrospun fibers [23].

Pyrolysis at elevated temperature is the next step to transform RF xerogels into carbon gels. The pyrolysis profile and temperature also affect the physiochemical properties of the final product, RF-derived carbon xerogel, which is an example of hard carbon.

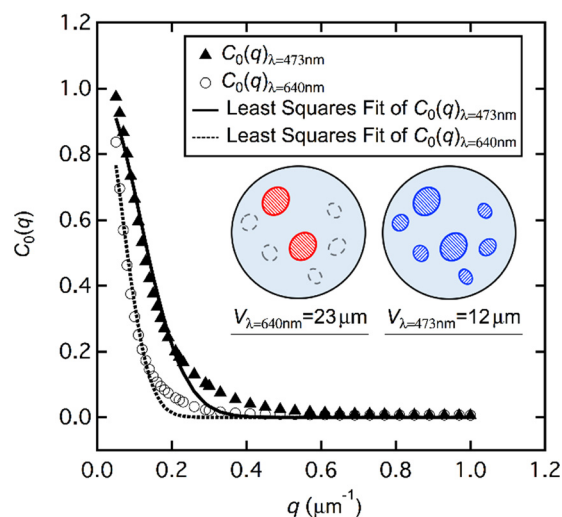


Fig. 5. Azimuthally averaged scattering intensity, $C_0(q)$, as a function of scattering vector, q , for a sample probed with two different wavelengths, 473 nm and 640 nm. The scattering intensity decays more slowly for samples with smaller grains. A larger average grain size is observed using the 473 nm light source.

As hard carbons are structurally compared as “house of cards” comprising randomly arranged graphene sheets, they allow adsorption of lithium ions other than only intercalation, RF-derived carbon xerogels were therefore tested for its electrochemical performance as an anode material for lithium-ion batteries.

RF xerogel in the form of monoliths and powder form exhibits lower specific capacity besides large irreversible capacity [15,16,24]. RF xerogel derived carbon thin films have also exhibited only moderate reversible capacity [25]. To address this, many strategies have been suggested such as activation or nanostructuring in recent past [26,27]. RF xerogel derived interconnected nanoparticles as obtained after repetitive sedimentation and inverse emulsion polymerization showed much improved reversible capacity which was stabilized at 385 mAh/g after 100 cycles of charge/discharge [27]. In another recent study, ball milled RF xerogel derived carbon nanoparticles also showed large reversible capacity, however, there was a significant capacity fade [28]. In yet another approach, RF xerogels were synthesized in the form of composites either by coating with SnO₂ or encapsulating SiO₂, SnO₂ nanoparticles in the matrix [16,24,29]. This improved initial capacity significantly, however, cyclic stability was poor in all these cases. Graphitization using transition metal (TM) as catalysts while synthesizing RF xerogel facilitated ordering of graphene layers that resulted in a much stable cyclic performance [30].

Thus, it is quite evident from the ongoing efforts about the potential of RF-derived carbon xerogels as promising alternative to graphite and other hard carbons used as anode for lithium-ion batteries, however, what still remains is to fully understand the structural and porous textural properties and correlate them with their electrochemical performance. This understanding will help in guiding the synthesis processes for more efficient anode materials for lithium-ion batteries in near future. As also suggested in a recent study by Job and coworkers [31,32], higher electrical conductivity, presence of wide pores, and low to moderate external surface area of carbon xerogels may address the large irreversible capacity and thus positively influence the electrochemical performance of these materials. Activation other than engineering RF sol chemistry to tailor the microstructure combined with doping of foreign elements like nitrogen and higher temperature treatment including graphitization may be the key factors for the best performance of these materials.

4 Nanostructured Carbon in Li-Ion Battery

In the past few years, carbon nanotubes (CNTs) and graphene, either as individual components or as composites with

nanostructured Si or different oxides (Sn-oxide, Ti-oxide, etc.), have demonstrated excellent gravimetric capacity, energy density, and capacity retention ability [33,34]. It was shown by Lahiri et al. that multiwall carbon nanotubes (MWCNTs), directly grown on copper current collectors, have excellent specific capacity, stability, and cycling ability [33] (Fig. 6). Moreover, these directly grown MWCNTs were demonstrated to have better adhesion with the current collector [35], making application of organic binders irrelevant and improving device life time. However, as discussed earlier, factors like reversibility, cycle life, and shape of the battery emerge out as vital issues. It is important to note that reversibility and cycle life of most CNT [33] or graphene based batteries are good.

Apart from these factors, future research directions in energy storage would be highly influenced by the type of application and properties required for any particular use. A battery used in electric vehicle (EV) and plug-in hybrid electric vehicle (PHEV) should deliver at least 16 kWh energy [36] and thus, factors like total weight and size of the battery become important issues. These factors can be optimized through proper design, high packing density electrode material, higher electrode thickness, new battery architecture, and obviously minimizing the cumulative weight of current collectors, electrolyte, separator, binder, connectors, packaging, and safety features. Carbon appears to be in a favorable position as carbon could offer almost similar gravimetric and volumetric capacity [34]. However, nanostructured carbon

is poor in packing density and scalable production is often an issue. Hence, new research should focus on these two critical issues. The issue of packing density can be addressed in quite a few diverse ways, e.g., by incorporating thicker battery electrodes, without restricting kinetics and conductivity of the battery [37]; compositing high-capacity nanostructured materials (e.g., Si, SnO₂, etc.) with CNT or graphene [38], and three-dimensional architecture [39–41]. Kang et al. have demonstrated the benefit of introducing three-dimensional architecture of MWCNT-based electrode in offering improved capacity (Fig. 7). These approaches, either individually or collectively, have huge potential to overcome the limitations of today's CNT or graphene electrode based Li-ion batteries.

New methods also need to be developed to achieve sufficient packing density for high-energy applications. New architectures (e.g., 3D electrodes, scoop, scaffold, or porous structures), novel synthesis techniques to grow high density CNTs, and design considerations like preparing novel composites of CNT/graphene with optimized quantity of nanostructured oxides or silicon could offer attractive properties and help us to reach the goal. In all the high-energy applications, scalability of electrodes to industrial level is an important factor and needs to be demonstrated to have real impact on future energy storage technologies. With these integrated approaches, it might be possible to reach to a more efficient and versatile energy storage platform, using nanostructured carbon based materials systems.

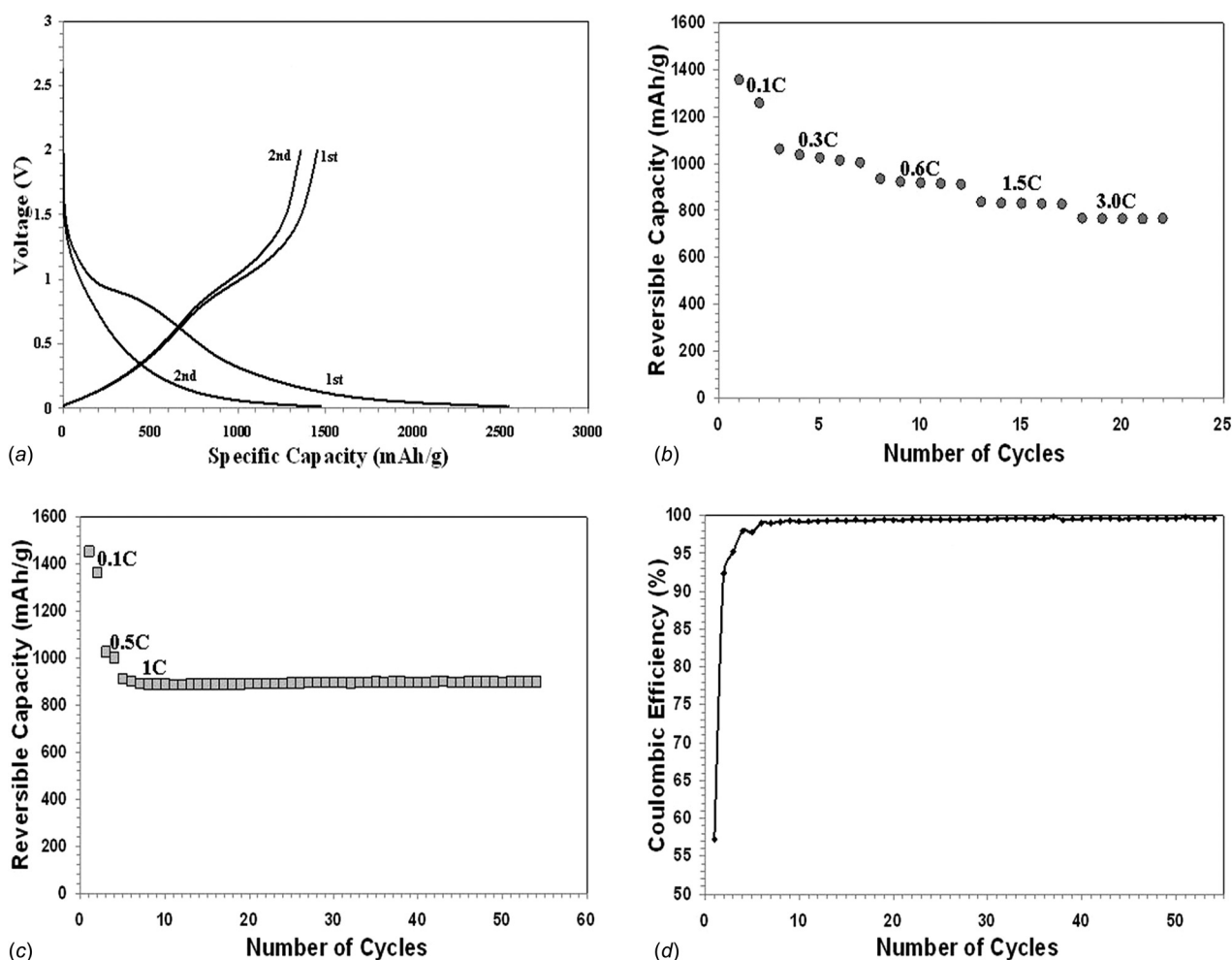


Fig. 6. Electrochemical characteristics of MWCNT-based anode: (a) charge–discharge performance in first two cycles, (b) rate capability, (c) stability, and (d) Coulombic efficiency of the MWCNTs grown directly on copper current collector. (Reprinted with permission from Lahiri et al. [33]. Copyright 2010 by American Chemical Society.)

5 Lithium–Manganese Rich (LMR-NMC)-Based Cathodes for High-Energy Density Lithium-Ion Batteries

The U.S. Department of Energy (DOE) and United States Advanced Battery Consortium (USABC) 2020 vision documents predict that the next generation lithium-ion batteries should have almost double the energy density (235 Wh kg^{-1}) of the currently available lithium-ion batteries based on lithium transition metal oxides, olivine cathodes, and graphite anodes for electric vehicles [42]. The batteries should have also reduced cost, improved safety, and cycle life. State-of-the-art lithium-ion cells use layered transition metal (TM) oxides (LiCoO_2 , $\text{LiNi}_{1/3}\text{Mn}_{1/3}\text{Co}_{1/3}\text{O}_2$ (NMC), or $\text{LiNi}_{0.8}\text{Co}_{0.15}\text{Al}_{0.05}\text{O}_2$) or phosphates (LiFePO_4 and LiMnPO_4) and Mn-based spinels (LiMn_2O_4 and $\text{LiMn}_{1.5}\text{Ni}_{0.5}\text{O}_4$) as cathodes and graphitic carbon as anode. The nominal capacity of most of these cathodes ranges between 140 and 180 mAh g^{-1} when cycled up to 4.2 V [43,44]. This is only half the specific capacity of graphite anode (372 mAh g^{-1}). Thus, there has been an intense research activity during the last decade to develop high-capacity or high-energy cathodes and anodes for lithium-ion batteries [43,44].

Lithium and manganese rich TM oxide composite cathodes are given by the generic formula, $x\text{Li}_2\text{MnO}_3 \cdot (1-x)\text{LiMO}_2$ (LMR-NMC) has almost double the capacity (300 mAh g^{-1}) of layered TM oxides but needs to be electrochemically cycled to a voltage $>4.4\text{V}$ to achieve this high capacity [44–55]. The high capacity is achieved by activation of Li_2MnO_3 component above 4.4 V forming Li_2O and MnO_2 [46]. This contributes to the high irreversible capacities of $>25\%$ for LMR-NMC electrodes. Besides, LMR-NMC electrodes have the limited capacity retention upon prolonged high voltage ($>4.4\text{V}$) cycling, due to significant reduction in the electronic conductivity [47–49]. The insulating surface films are formed on the electrode surface because of electrolyte decomposition and reaction products [48]. Besides, LMR-NMC cathodes suffer from poor electronic as well as ionic conductivity, which contributes poor rate or power capability of LMR-NMC and capacity fade. The capacity fade is also associated with Mn dissolution from the host structure upon continuous high voltage cycling. Besides, the electrochemical stability of carbonate-based electrolyte with LiPF_6 salt will be a serious concern that can sustain high voltage cycling (up to 5 V). LMR-NMC primarily belongs to an $\alpha\text{-NaFeO}_2$ structure (O3 structure) with a small monoclinic phase (C2/m), originating from the Li^+ ion ordering in the transition metal layer. During high voltage cycling $>4.4\text{V}$,

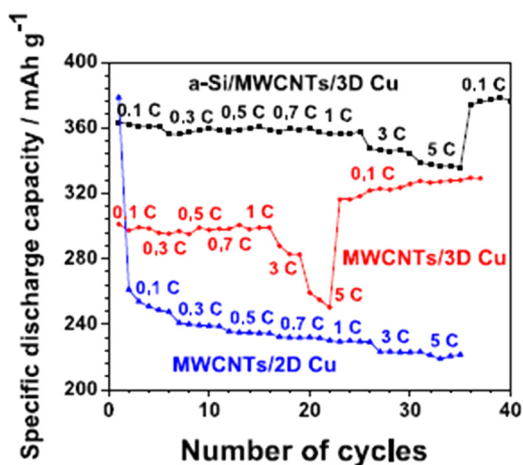


Fig. 7 Effect of three-dimensional electrode design on the capacity of CNT-based Li-ion battery anode (MWCNTs/2D Cu: MWCNTs on copper foil; MWCNTs/3D Cu: MWCNTs on copper foam; and a-Si/MWCNTs/3D Cu: amorphous Si-coated MWCNTs on copper foam). (Reprinted with permission from Kang et al. [41]. Copyright 2012 by Elsevier.)

LMR-NMC undergoes a structural transition from layered to the spinel phase when continuously cycled at above 4.4 V [47–50] resulting in significant loss of energy. The loss of energy is due to significant voltage fade, i.e., discharge profile gradually moving below 3 V plateau from 3.8 V when cycled >100 times [50]. During cycling, practical energy density of LMR-NMC cathodes is reduced from 1000 Wh kg^{-1} during initial cycles to $\sim 750 \text{ Wh kg}^{-1}$ during the 100th cycle upon subsequent cycling which makes LMR-NMC practically impracticable.

Researchers at the Argonne National Laboratory, Lemont, IL, have extensively worked on LMR-NMC cathode material. The researchers have conducted many fundamental and experimental studies in order to improve the performance of the LMR-NMC. Besides, researchers at the Oak Ridge National Laboratory (ORNL), Oak Ridge, TN, have thoroughly worked in this material in order to improve the electronic conductivity and interfacial stability of LMR-NMC. Researchers at ORNL found that carbon nanofiber (CNF) and nanotubes graphene additives into the active mass improve the capacity, cyclability, and rate capability, because CNFs provide an effective electronic wiring around the surface of the LMR-NMC forming an interconnected conducting pathway across the bulk of the electrode despite the formation of a surface passivation films due to electrochemical cycling [47–49]. The cells can retain capacities $>80\%$ of the original capacity around 500 charge–discharge cycles in coin type cells.

Besides, improved electrochemical performance of LMR-NMC can be obtained by a nanometer layer coating of lithium conducting solid electrolyte, such as lithium phosphorus oxynitride (lipon) [49] on to LMR-NMC. Studies show that a few nanometers thick lipon film is very effective toward improving the interfacial stability against high voltage cycling leading to better high-rate performance, cycle life, and higher useable capacity [49]. Besides, there are many studies on Al_2O_3 , RuO_2 , TiO_2 , AlPO_4 , CoPO_4 , AlF_3 , LiFePO_4 , LiV_3O_8 , $\text{Li}_4\text{Mn}_5\text{O}_{12}$, VO_2 , etc., surface coatings in order to improve the interfacial stability and cyclability [50–55]. Although the surface coatings or conducting diluents improve the rate performance and cycle life to some degree in relation to pristine LMR-NMC but it cannot address issues of voltage fade or suppression of the discharge profile which gradually moves to below 3 V plateau when cycled >100 times as shown in Fig. 8.

The structural transition to the spinel phase is an intrinsic/bulk phenomena associated with transition metal ions that migrate to the lithium layer during high voltage cycling ($>4.4\text{V}$). The migration takes place because of vacancies created by oxygen release as Li_2O from Li_2MnO_3 component during high voltage cycling. Because of migration, the layered structure slowly transforms to spinel during the course of cycling due to which there is decay in the voltage plateau from 3.8 V region to 2.8 V region which decreases the energy density.

So, it is necessary to move away from Mn rich phase and revisit the transition/alkali metal compositional space. There may be possibility that isovalent doping with transition metal/alkali ion such as Cr and Mg will stabilize the structure, may prevent structural transformation, and could lead to capacity drop. Besides, F-substitution or coating helps in the improvement of electrochemical performance at high cut-off voltages, improves thermal stability, and reduces charge transfer resistance. Many researchers have postulated that substituting oxygen by fluorine is an highly advantageous method to improve electrochemical performance. F-doping in $\text{LiNi}_{0.5}\text{Mn}_{1.5}\text{O}_4$ (NMS) resulted in improvement of electrochemical performance like increase in initial capacity and high-rate capability $\sim 10\%$ and also shows better thermal stability [56]. Manganese dissolution is also reduced ($\sim 30\%$), as electrode surface is less prone to HF attack. In general, 2–5% of fluorine is recommended for best electrochemical performance of Li-ion cells.

Here, at the Indian Institute of Technology (IIT) Hyderabad, Hyderabad, India, we are extensively focusing on cation (Mg, Cr, etc.) and anion dopings, such as fluorine to stabilize the interface.

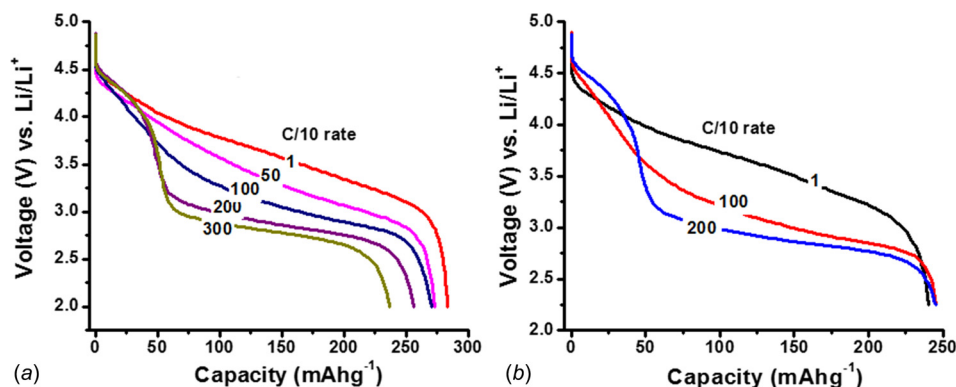


Fig. 8 Cycling behavior at C/10 rates of charge–discharge for the (a) 1 h and (b) 3 h lipon-coated Li-rich NMC composite electrodes (as indicated) in the potential range 2.0–4.9 V, in ethylene carbonate-dimethyl carbonate (EC-DMC) 1:1/LiPF₆ 1.2 M solutions at 25 °C. Cycling protocol was constant current–constant voltage providing potentiostatic steps at desired higher cut-off potential until the current reaches value of C/50. The lower cut-off potential was 2.0 V versus Li/Li⁺. The discharge profiles for the 1 h and 3 h lipon-coated LMR-NMC composite electrodes move to lower voltage (2.8 V) plateaus showing significant loss of energy. (Reprinted with permission from Martha et al. [49]. Copyright 2013 by Royal Society of Chemistry.)

Moreover, F-coating or doping partially replaces M–O bonds with M–F bonds on the surface [54,56]. The M–F bond is stronger and thus stabilizes the structure during cycling. F[−] doping in LMR-NMC delivers high capacity (10–20% greater than conventional electrodes), ~300 mAh g^{−1} at C/10 rate, and have high discharge plateau voltage and low charge plateau voltage compared to conventional electrodes (Fig. 9). More than 200 mAh g^{−1} capacity is obtained below 4.4 V for F-doped LMR-NMC compared to the conventional electrodes where ~200 mAh capacity is obtained >4.4 V. Results indicate that F-doped LMR-NMC cathodes stabilize structure and reduce the voltage drop, thereby reducing energy loss along the cycles.

Beside, we stabilize the layered LMR-NMC structure by simultaneous doping with trivalent Cr³⁺ and divalent Mg²⁺ at Ni site or with both cation and anion dopings at Ni and oxygen sites, respectively. Cation doping increases the average oxidation state of Mn, thereby reducing Jahn Teller distortion and dissolution. Beside, cation dopings reduces the migration of metal ions from octahedral site (Oh) to the surface through the tetrahedral site (Th), thereby increases structural stability and significantly reduces energy loss during the prolonged cycling.

It is believed that the study will open a new realm of possibility for LMR-NMC cathode material which has almost double the capacity of currently available cathodes and could be the possible cathode material for next generation lithium-ion batteries.

6 Three-Dimensional Imaging Challenges in Li-Ion Batteries

Enhancing the performance (e.g., simultaneously thermal, mechanical, and electrochemical function) of materials whose microstructures consist of structural networks relies on a well-tuned microstructural economy. In order to understand structure–property relationships in these materials, it is essential to characterize the features of their microstructural networks that directly influence the density of active sites as well as the efficiency and robustness of transport pathways. A body of literature is emerging that is focused on the development of 3D imaging techniques for the characterization of materials whose performance depends upon distinctly complex microstructural features [57]. In surveying these works, authors commonly cite several motivating factors for direct 3D imaging. These factors are detailed below with specific examples relevant to Li-ion batteries highlighted.

Three-dimensional imaging provides a means to directly observe a material’s heterogeneity/anisotropy, which, using established techniques, is quantifiable only in abstraction. In other

words, the use of 3D imaging methods affords the investigator the invaluable ability to identify the specific features that contribute to a structure’s heterogeneity/anisotropy. For example, in the characterization of a Li-ion battery’s negative electrode by Shearing et al. [58], the group found that the structure’s tortuosity, porosity, and volume-specific surface area were highly heterogeneous in three dimensions. Such studies exemplify how 3D imaging can complement microstructural characterization results provided by established techniques in a powerful way, which, in the future, could inform the rational design of materials with highly reticulate microstructure.

Three-dimensional shape influences material performance in at least two ways: (a) it establishes driving forces that initiate material phenomena [59] and (b) it dictates the manner in which microstructural networks aggregate, i.e., the microstructural economy. A highly complex geometry can be characterized by its local curvature distribution, which provides a means of visualizing the frequency of various interface shapes within a structure [60].

Three-dimensional imaging can also offer a means for validating models that make use of stochastic structures such as those based on sphere packing. For example, Thiedmann et al. [61] assessed the validity of their stochastic model of the Li-ion battery’s negative electrode microstructure using 3D images obtained by X-ray microtomography, which was performed by Shearing et al. [58]. The group found that the geometric tortuosity of

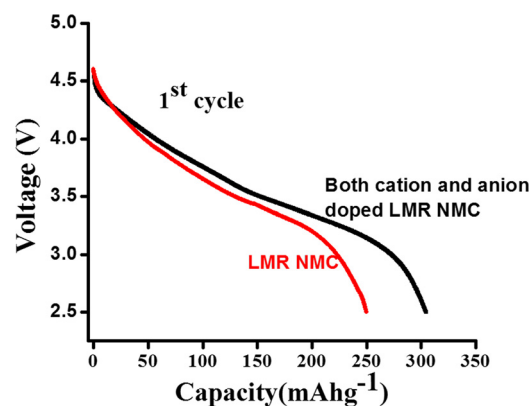


Fig. 9 Voltage profiles for the LMR-NMC and doped cathodes during first cycle. Doped cathodes deliver 20% more capacity than pristine LMR-NMC cathodes and have high plateau voltage.

structures generated by the model differed significantly from that of the actual structure. This observation is important because tortuosity directly relates to the electrode's ability to efficiently transport lithium and is therefore relevant to its performance.

Three-dimensional imaging of Li-ion batteries can be performed using a variety of techniques, including X-ray tomography and focused ion beam-scanning electron microscopy (FIB-SEM) [57]. FIB-SEM serial sectioning involves the imaging (by SEM) and then milling away (by FIB) of successive, closely spaced slices of material to obtain a series of micrographs, which, when aligned and stacked, form a 3D image of the material's microstructure. Chemical detection can be achieved by exploiting secondary electron contrast using an Everhart-Thornley (ET), in-lens or energy selective backscattered (ESB) electron detector.

X-ray tomography is a transmission X-ray microscopy (TXM)-based technique that can be used to map three-dimensional structures at the micro- and nanoscales [62]. For example, a surface-meshed structure of a lithium cobalt oxide cathode from [63] is shown in Fig. 10. When applied with a synchrotron X-ray source, this technique is capable of spectroscopic chemical detection. Specifically, the ability to tune the energy of the X-rays provided by a synchrotron enables the collection of tomographic images across the elemental absorption edges of the sample's components/phases. The characteristic contrast difference exhibited by particular elements/chemical species in images collected at various points across the absorption edge then permits elemental and/or chemical mapping of the sample [64,65]. By segmenting the images collected across an absorption edge (or multiple absorption edges), a digital representation of the structure with discrete labels for each of the material's elemental and/or chemical components (plus pore space) is obtainable. Subsections of the segmented structures, termed "representative volume elements" (RVEs), are then extracted and characterized computationally [66,67] using a variety of algorithms [68,69].

An array of properties can be calculated from segmented 3D images of a material's microstructure [68,69], i.e., from digital representations of the microstructure with each phase labeled by a discrete value. For example, a size distribution is obtained as described in detail in Ref. [70]. Interface area can be measured by scanning through the structure in three dimensions, counting and classifying voxel faces across which a label change is detected. Connectivity (sometimes used in the literature interchangeably with "contiguity") can be measured using a numerical painting scheme as described in Ref. [71]. Three-dimensional measurements of each phase's contiguity make possible the specification of "connected" interface area and reaction site density, i.e., areas and boundaries that are connected by continuous pathways to the volume's exterior. These areas and boundaries are most relevant to performance because they represent active sites that belong to a

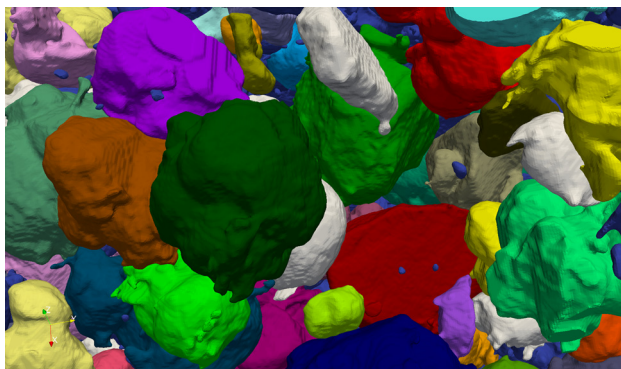


Fig. 10 Three-dimensional imaging of lithium cobalt oxide cathode material using X-ray tomography. The colors (online) represent lithium cobalt oxide particles that have been individually surface-meshed. (Reprinted with permission from Roberts et al. [63]. Copyright 2016 by ASME.)

connected network. Tortuosity measurements, which describe the twistedness or windiness of transport pathways, will be based on solutions to the Laplace equation within 3D domains of each material component obtained directly from TXM or FIB-SEM images [72].

Local curvature measurements [73–76] are useful in characterizing the complex geometries exhibited by reticulate microstructures. Measurements of 3D curvature require first the generation of meshes on each phase's surface. Typically, quadric surfaces fitted locally over groups of triangles known as surface patches are solved for their eigenvalues, from which the local surface normal vector as well as the principle, mean, and Gaussian curvatures can be computed (this approach is used, for example, in the software AVIZO [77]). For analyses, local mean, Gaussian, and principal curvature measurements can be summarized into probability density distributions (weighted by each surface patch's area). The probability density distributions provide information about the spectrum of interface shapes that occur over the surface [59].

Primary factors relevant to the performance of the LiMnO_2 cathode include the rate of Li transport in LiMnO_2 and the material's electronic conductivity. Visualization of the 3D network may be beneficial to obtain fundamental insight necessary to enhance electrochemical reactions, reduce capacity loss, and enhance ion diffusion [78,79].

7 Thermal Transport Modeling

Thermal transport in Li-ion batteries continues to be an important area of research, with direct applications on the performance, safety, and reliability of energy conversion and storage devices. Fundamentally, heat generated during charge or discharge due to Ohmic and non-Ohmic mechanisms must conduct through the various materials and material interfaces within the cell before being convected to the ambient from the outer surface of the cell. Both heat generation and heat conduction processes must be analyzed in an integrated fashion, also considering the interaction of these processes with other transport phenomena, such as electrochemical and charge transport.

Thermal processes in a Li-ion cell occur over multiple length-scales starting from the atomistic scale, through the scale of electrode materials all the way to large-sized energy storage devices [80]. The multiscale nature of thermal transport necessitates the consideration and analysis of heat transfer processes at each of these scales as well as the development of multiscale thermal models. Empirical or semi-empirical models may be relevant and useful for representing detailed heat transfer characteristics into equations that are more readily usable in real-time applications. The following subsections list key research needs in the modeling of thermal transport at each lengthscale relevant for the analysis of Li-ion cells.

7.1 Atomistic-Level Thermal Transport Modeling. A variety of molecular dynamics (MD)-based approaches have been used for atomistic-level modeling of thermal transport through materials and interfaces of relevance to engineering applications [81–83]. However, there is a lack of work on MD simulations for thermal transport through electrochemical materials and interfaces. It is critical to apply existing tools and develop new ones for analysis of heat transfer in electrochemical systems. Such tools need to be computationally optimized in order to compute coupled thermal and electrochemical transport. Constitutive relationships that connect the two transport processes need to be developed for such simulations. Insights into the nature of thermal transport at the atomistic scale in electrochemical materials must be integrated with electrochemical transport and eventually with manufacturing and assembly. This will aid in optimization of materials for future Li-ion and other battery chemistries. It is critical for such tools to be used early in the materials discovery process, so that materials with co-optimized thermal and electrochemical transport characteristics may be developed. This is particularly important for

high-rate applications where large amount of heat generation is expected.

Since atomistic modeling techniques can only handle a small number of molecules, it is important to develop reduced-order models based on detailed MD simulations that can be used as an input for thermal computations at larger lengthscales.

7.2 Material-Level Thermal Transport. Thermal transport through Li-ion battery materials is a considerably complicated process due to several reasons. Typically, Li-ion electrodes are a heterogeneous mixture of multiple materials including the active material, binder, etc. The nature of thermal transport through these individual materials is not well known. Further, the nature of thermal transport through mixtures of these materials is also largely unexplored. It is important to develop analytical models for predicting thermal conductivity of such heterogeneous systems. In conjunction with electrochemical models, such thermal models may aid in multiphysics codesign and co-optimization.

Another key research direction at this scale is the development of analytical heat transfer models to be used in conjunction with experiments for the measurement of thermal properties of electrode and other materials of relevance to Li-ion cells. Due to the thin and heterogeneous nature of electrodes, thermal property measurement is challenging. Further, in situ measurements present additional difficulties, due to which the development of new measurement methods aided by analytical model development is critical, particularly for the characterization of heat transfer in new Li-ion and other cell chemistries.

In addition to materials, material interfaces at the scale of electrodes also play a key role in thermal transport [84]. The dominance of interfacial thermal transport is not entirely surprising, but this has not been investigated much in the context of Li-ion cells. While some work has suggested that a large portion of total thermal resistance occurs at interfaces in a Li-ion cell [84,85], a detailed study of the various factors affecting thermal transport at interfaces is missing. Theoretical and numerical models are needed for understanding how interfacial thermal transport is affected by the electrochemical ambient, nature of surfaces, and the presence of intermediary molecules. Such theoretical models need to be integrated with experimental measurements for validation and development of design tools for end-use.

Finally, at the scale of electrodes, analytical heat transfer models must be used for examining the relationship between manufacturing, assembly, and thermal performance. A theoretical and/or numerical study of such processes will help develop an understanding of these relationships, and hence of the optimization of manufacturing and assembly to obtain thermally optimized electrode materials and assemblies.

7.3 Cell-Level and System-Level Thermal Transport. At the lengthscale of single cells and battery packs, thermal transport is governed by well-known energy conservation equations that can be solved to determine the temperature field either analytically when possible [86,87], or in the case of more complicated geometries, in a numerical fashion, for example, using finite element simulation tools. Analytical solutions can be easily computed and integrated with other battery management tools, whereas finite element simulations typically need to be carried out in separate, commercial software that are difficult to integrate. Due to these advantages, a shift away from finite element simulations should be explored. Real-time computation of temperature field in a single cell or in a battery pack will directly enable proactive, thermally smart battery management to maximize performance and prevent undesirable scenarios such as thermal runaway.

Due to the large scale and complexity of cells and battery packs, detailed thermal modeling is often not possible, in which case, reduced-order models and parameterized models offer a compromise between computation time and accuracy. These tradeoffs need to be studied in detail in the context of heat transfer

computation for large electrochemical systems. Novel approaches for thermal parameterization of complex geometries will help develop rapid thermal computation tools for cells and battery packs.

There is also a need for developing analytical models for studying the effect of various thermal management strategies for cooling large electrochemical systems [88]. Specifically, theoretical models for development and optimization of advanced thermal management techniques, such as liquid cooling and two-phase cooling, are needed.

The modeling of long-term, thermally driven aging and reliability of cells and battery packs is also needed. Such models that have been developed extensively for other engineering applications could also be useful in understanding the factors that affect reliability of Li-ion based systems.

Finally, it is important to develop analytical thermal models for studying extreme events such as thermal runaway. Predictive tools for thermal runaway are expected to be critical for future battery management systems. Such analytical thermal tools will require close interaction with experiments, which will provide the values of various parameters needed for accurate thermal runaway prediction.

8 Time-Stepping Methods and Solvers for Battery Models

Wide range of phenomenon in different scales necessitates multiscale models for batteries. Models for batteries vary from empirical models to kinetic Monte Carlo (KMC) or atomistic models as shown in Fig. 11 [89]. In our view, at least pseudo-2-dimensional (P2D) models should be used for modeling Li-ion batteries. Anything less than that would mean a significant compromise on the accuracy and fidelity leading to overdesign and under-utilization of batteries to enable safer operation.

P2D models involve two spatial coordinates. There are various methods to discretize the spatial coordinates: finite differences [90,91], finite volume [92], and other collocation-based methods [93,94]. Different approaches have been pursued to efficiently simulate the battery models by using spectral methods (Galerkin-based collocation [93], orthogonal collocation on finite elements [94], orthogonal collocation with co-ordinate transformation [95], and reformulation in the solid phase [96–99]). Significant gain in CPU time is obtained by approximations in the pseudodimension (r) and liquid phase (x). Use of reformulated models for Li-ion battery control applications is discussed elsewhere [100]. In this section, we focus on numerical issues and approaches for simulating battery models in time domain. Battery models result in differential algebraic equations in time. First, different methods are classified and introduced.

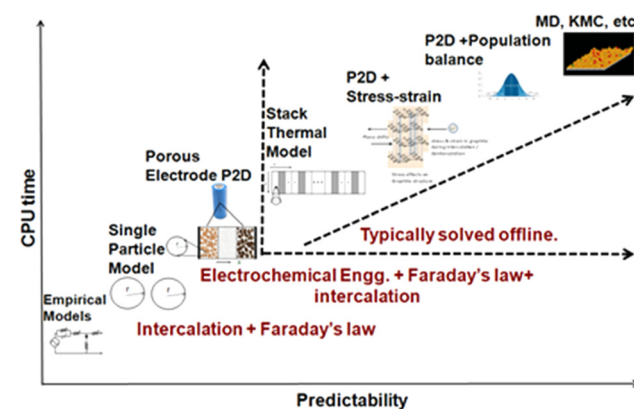


Fig. 11 Wide range of physical phenomena dictates different computation demands [89]

There are explicit and implicit methods to solve ordinary differential equations (ODEs). Battery models are stiff in nature and cannot be solved by nonstiff methods and stability of the numerical scheme is important. Numerical methods can be broadly classified as two types: (1) Runge–Kutta (RK) methods and (2) multistep methods. Instead of describing each of them separately, different numerical methods are introduced first and then analyzed. A scalar differential equation defined by $(dy/dt) = f(y)$. In particular, a simple example is given by $(dy/dt) = \lambda y$ with $y(0) = 1$. Index-1 differential algebraic equations (DAEs) arising from battery models are in the form $(dy/dt) = f(y, z)$; $0 = g(y, z)$, where y is a differential variable and z is an algebraic variable.

8.1 Euler Forward (EF) Method. This is probably the easiest method to implement. If the values of y are known, then the slope at $t=0$ is known and y_1 (at the next time step) is easily found. This way one can march forward easily in time.

8.1.1 Disadvantages. EF method is accurate to the only first order in time step, h . This means that very large number of steps are needed for simulating ODEs with this method. The order of accuracy can be increased by using higher order methods (for example, RK fourth-order method implemented as ODE45 in MATLAB [101]). When solving stiff ODEs, very small time step (sometimes even 10^{-15} or smaller) needs to be taken for simulating models in time from 0 to 1. EF method is stable only inside a small circle defined by $0 < h\lambda < 2$. Stability of EF methods can be studied by applying the method a single step to find the stability function R . EF method is not A-stable as the stability region does not cover the right-hand side of the complex plane [102].

EF method (and similarly all the explicit multistep and RK methods) cannot be directly used for DAEs. Even if y_1 is found from f_0 , z_1 needs to be found from the nonlinear algebraic equation which will require Newton Raphson iterations, thereby losing the advantage of being an explicit method.

8.2 Euler Backward (EB) Method. This method requires a nonlinear solver to find y_1 if f_1 is nonlinear. For a system of ODEs, even for a linear system, this will involve inversion of a matrix. Typically, direct inversion is avoided and efficient linear solvers are used to facilitate the Newton–Raphson method.

8.2.1 Disadvantages. Just like EF method, EB method is accurate to the only first order in time step, h , and requires Newton–Raphson approach for solving nonlinear algebraic equations arising from nonlinear ODEs or DAEs.

8.2.2 Advantages. Stability of EB methods can be studied by applying the method a single step to find the stability function R . EB method is both A-stable and L-stable and the most stable method. EB can be directly used for DAEs. This set of nonlinear algebraic equations can be solved for both y_1 and z_1 directly. Note that for EB method, the initial condition of z , z_0 is irrelevant and only serves as a guess for getting z_1 . While theory may exist for this statement, our experience suggests that if an optimization problem is solved (say maximize charge stored), EB method for discretization will never overpredict the objective. Other methods might converge faster, but at lower number of node points might overpredict the objective. Simulating models with EB method will at least give a qualitative estimate for optimization of index-1 DAEs. Without going to theory, it should be noted that EB method might damp out oscillations faster than reality.

8.3 Runge–Kutta (RK) Methods. Both EF and EB methods are accurate only to first-order. When solving an equation, we take half the step with EF method and get the value at the end of the first step called as the explicit midpoint method. One can show that this method is indeed second-order accurate. In general, RK methods can be conveniently represented by the Butcher tableau. Explicit methods are easy to implement (ODE45), however,

satisfying order conditions is difficult for higher order. They are not good for stiff problems. For implicit methods, order conditions are easy to satisfy. Note that implicit midpoint method (IMP) is also the Gauss Runge–Kutta method of order 2 (single stage). For a s stage Gauss method, one can get an order of $2s$ method. There are subtle variations between methods yielding the same stability function. An advantage of single step (RK methods) is that it is easy to adjust time steps for adaptive time-stepping integrators. For RK methods, it is not possible to increase the accuracy for DAEs beyond order 2 without increasing the number of variables solved. One can show that the RADAU IIA scheme of order 3 for the DAEs gives third-order accuracy for both y_1 and z_1 , but we double the number of variables to solve. There are ways to get more than second-order accuracy without increasing the number of variables. One such method is backward differentiation formula (BDF) method, more details can be obtained elsewhere [103]. This algorithm is implemented in various solvers, such as DASSL [104], DASPK [105], and IDA [106]. Note that BDF methods have great stiff decay property enabling them as a good choice for DAEs and stiff models. However, BDF methods (and any multistep) methods are A-stable only up to order 2. When adaptive solvers are implemented in production codes that are used, error estimates are obtained often times using an inferior estimate in terms of stability. Adjusting the step size restricts stability criterion for BDF methods.

The key features of some of the methods are discussed in a tabular form for easier comparison and are summarized in Table 1.

Other methods of relevance include diagonally implicit Runge–Kutta (DIRK) [107], MEBDF [108], mono-implicit Runge–Kutta (MIRK) [109], and second derivative methods.

Even when we have good solvers in time, unknown initial conditions for z variables might stop the solver from simulation. An example of a two equation system representing a thin film nickel hydroxide electrode described in [110] is studied during the charging process. This system can cause difficulty in determining consistent ICs [111]. When deviating from the consistent ICs, many initialization routines and solvers fail to obtain a solution [112], which shows the range of possible ICs for the algebraic variable that provide a solution for different solvers and approaches including the proposed single-step approach.

9 Critical Issues in Identifying Ideal Electrolytes for Lithium Batteries: An Atomistic Perspective

Transformative changes are required in battery technology for addressing current challenges in advanced electric vehicles [113–119]. In particular, the requirements to develop safe, low-cost battery of sufficient energy storage capability have catalyzed a wide range of research efforts to both improve existing lithium-ion (Li-ion) batteries as well as to explore novel chemistries such as in lithium–sulfur (Li–S) batteries [120,121]. Regardless of the specific chemistry, one of the common challenges remains identifying an electrolyte with high ionic conductivity, robust thermal and electrochemical stability, and low vapor pressure to allow for safe operations. Various research efforts have been directed toward identifying novel electrolytes, based on ionic liquids, glymes, sulfones, nitriles, polymers, and gels, to name a few [122]. These electrolytes have several promising properties, and in conjunction with additives, can serve as excellent electrolytes in lithium batteries. However, electrolytes are often incompatible with high capacity and high voltage electrodes that are presently being developed in order to enhance energy densities of batteries for automobile applications. In particular, using electrolytes in high voltage lithium cells requires wide electrochemical stability windows to maintain improved performance over several charge–discharge cycles. Additionally, formation of optimal solid-electrolyte interphase (SEI) layer and low interface impedance are very important aspects in developing robust batteries [123]. Therefore, developing enhanced electrolytes should go hand-in-hand with designing novel electrode materials in order for

Table 1 Comparison of different numerical techniques for time stepping for DAEs

Method	Explicit/Implicit	RK/Multistep	Stability function	Order of accuracy	Software codes/solvers
Euler forward	Explicit	RK/MS	$1 + z$	$y: O(h), z: NA$	
Euler backward	Implicit	RK/MS	$\frac{1}{1+z}$	$y: O(h), z: O(h)$	ODE15s (max order 1) and DASSL (order 1)
Implicit midpoint	Implicit	RK/MS	$\frac{1+z/2}{1-z/2}$	$y: O(h^2), z: O(h)$	NA
Trapezoidal	Implicit	RK/MS	$\frac{1+z/2}{1-z/2}$	$y: O(h^2), z: O(h^2)$	
RadauIIA (order 5)	Implicit	RK	$\frac{1 + \frac{2}{5}z + \frac{1}{10}z^2}{1 - \frac{3}{5}z + \frac{3}{10}z^2 - \frac{1}{10}z^3}$	$y: O(h^5), z: O(h^5)$	RADAU5 [102]
BDF	Implicit	MS	Depends on the number of steps	A-stable only up to order 2.	DASSL [104], IDA [106], and ODE15s (MATLAB)
Rosenbrock ^a	Semi-implicit	MS	Depends on the number of stages	1–5 for y and z Order dependent on the number of stages A and L stable third order possible with three stages	M. Roche [117]

^aDAEs with Rosenbrock methods need exact initial conditions for AEs to start with, unlike BDF and Radau methods.

these components to be compatible. Given the wide variety of electrode structures that are currently being explored, developing compatible electrolytes purely on an experimental basis will require extensive trial-and-error efforts that are both expensive and time-consuming. Therefore, an integrated experimental and theoretical modeling approach, particularly at the molecular scale, will be extremely effective in designing molecularly tailored electrode–electrolyte interfaces that enhance electron transfer, reduce interface impedance and dendritic growths, and improve chemical and electrochemical stability.

Safety is one of the critical aspects in developing improved lithium batteries. The safety concerns are directly related to the high vapor pressure of currently used electrolytes based on organic liquids. Therefore, a wide range of liquid and solid electrolytes based on ionic liquids, glymes, sulfones, nitriles, ceramics, polymers, and gels are currently being explored as alternate electrolytes [122]. Reviewing the modeling work that has been reported for all these classes of electrolytes is beyond the scope of this article. Therefore, we pick ionic liquids as model chemical species and discuss various aspects of atomistic modeling that can help with selection of ionic liquid based electrolytes [124]. Unlike conventional electrolytes, ionic liquids are nonhazardous, have low vapor pressures, and are nonflammable, and are therefore suitable candidates for electrolytes in lithium batteries [125,126]. Furthermore, the physicochemical and electrochemical properties of ionic liquids can be tailored by combining cations based on aromatic and saturated cyclic amines, sulfonium ($[R_3S]^+$), tetralkylammonium ($[R_4N]^+$), and phosphonium ($[R_4P]^+$) groups, where R represents alkyl groups, with inorganic and organic anions such as hexafluorophosphate ($[PF_6]^-$), tetrafluoroborate ($[BF_4]^-$), $[CF_3CONCF_3SO_2]^-$, and $[N(CF_3SO_2)_2]^-$ [127]. Developing structure–function relationships is extremely important to efficiently screen ionic liquid based electrolytes with desired properties, as illustrated in the schematic in Fig. 12 [128]. Another route for tuning properties is through use of additives.

Here, we review N-methyl-N-propylpyrrolidinium bis(trifluoromethanesulfonyl)imide (mppy⁺ TFSI⁻) ionic liquid [129], which has been widely explored as potential battery electrolyte. One of the major disadvantages of this electrolyte is that it has a relatively low ionic conductivity. Strong coordination of Li⁺ with TFSI⁻ ions [130] results in the occurrence of negatively charged clusters in the homogeneous and isotropic ionic liquid [131], which leads to reduced mobility of Li⁺ [130] that lowers the

overall ionic conductivity of the electrolyte. Various research efforts have attempted to synthesize low viscosity ionic liquids with improved ionic conductivity [132,133]. Another relatively simple route to address this issue is to include small amounts of molecular additives that can improve the transport properties of ions [130] as well as help form an SEI layer [134]. Several research efforts have studied organic additives [135] to improve the properties of ionic liquids [136] while maintaining their non-flammability characteristics [137]. Molecular simulation methods, such as molecular dynamics (MD), directly account for interactions between the various ions and molecules and are therefore very effective in evaluating diffusivity of ions within electrolytes comprising mixed ionic liquid-additive systems. For instance, MD simulations reported by Deshpande et al. have shown that small amount of ethylene carbonate additive is extremely effective in enhancing the ionic conductivity [138]. Radial distribution functions of lithium ion with respect to the atoms of the ionic liquid anion and additive molecules indicated that the negative charges on the oxygen atoms of the additives reduce the formation of negatively charged clusters by preferentially coordinating with Li⁺ ions. Of the additives simulated, ethylene carbonate, due to its highly electronegative oxygen, is the most effective in reducing the coordination between Li⁺ and TFSI⁻. The self-diffusion coefficient of Li⁺ is increased by around 249%, in the presence of ethylene carbonate at 0.2 mole fraction, when compared to that of pure ionic liquid electrolytes. These results are in agreement with Raman spectroscopy based study that also indicated reduced association of Li⁺ with the anion of ionic liquids [130] when ethylene carbonate or vinylene carbonate is added. Further studies based on MD simulations, including those of interfaces, rely on the development of reliable force fields.

High current density is another requirement for improved performance of batteries. In particular, the current density at the anode is directly dependent on the rate constant for the electron transfer reaction as evident from the Butler–Volmer equation [139–141]. Lithium metal is oxidized at the anode during the discharge cycle producing positively charged Li⁺ ions [142], $Li \rightarrow Li^+ + e^-$, while the reverse reaction happens during charging [143]. Even though the molecular structure of electrolytes has profound impact on the kinetics at the electrode–electrolyte interface, very few modeling based studies have investigated the effect of electrolytes. As part of a recent study, Kazemiabnavi et al. performed first principles calculations to investigate the effect of

ionic liquid based electrolytes on the electron transfer rate [144]. In order to correlate the chemical structure of ionic liquids with the reaction kinetics, the rate constant for electron transfer was calculated in the presence of 1-alkyl-3-methylimidazolium ($C_n\text{MIM}^+$) TFSI $^-$ ionic liquids with varying length n of the side alkyl chain. The transition state theory (TST) [145] and other variants of TST [146–148], widely applied for calculating chemical reaction rates, are not viable since characterizing the transition state in this type of reactions is not straight-forward. Therefore, Banerjee et al. applied the Marcus theory [149,150] to evaluate the rate constant using calculated thermodynamic parameters, such as the inner and outer sphere reorganization energies, Gibbs free energy, and the electronic coupling energy. The first ionization energy and vaporization energy of lithium calculated from density functional theory (DFT) matched with the experimental values very well. The calculated Gibbs free energy of the overall reaction decreased linearly with the inverse of the static dielectric constant of the ionic liquid which in turn corresponded with increase in the length of alkyl side chain of the ionic liquid cation. Consistent with this trend, the electron transfer rate constant was seen to increase with decreasing size of the alkyl side chain on the imidazolium cation. The electron transfer rate at the cathode–electrolyte interface has also been calculated using similar theoretical approach [151].

In conclusion, prior work on modeling ionic liquids demonstrates that atomistic simulations are powerful tools that can be used for screening electrolytes as well as to provide detailed insight into the fundamental mechanisms that govern the kinetics and thermodynamics of charge transfer and transport through electrolyte and electrode–electrolyte interfaces. Ab initio quantum mechanical methods as well as classical MD have been employed for studying electrochemistry and transport at various length scales. However, there are some key issues that still need to be addressed and atomistic simulations can play a valuable role. In particular, disruptive improvement in performance can only be attained through concerted efforts to design novel electrode architecture and identify compatible electrolytes. While recent studies have modeled chemistry at the electrode–electrolyte interface including the growth of the SEI layer, additional work is necessary to completely understand the influence

of chemistry on the mechanics of dendrite growth and ion transport through the SEI layer of realistic composition. Furthermore, determining interface impedance for a wide range of electrode–electrolyte combinations can be extremely valuable in developing lithium batteries with significantly improved energy densities. It is noteworthy that further efforts in developing reactive and polarizable force fields are necessary to access larger length scales through classical MD simulations. Finally, close collaboration between modeling and state-of-the-art experimental characterization is required to study the complex phenomena described above.

10 Microstructure–Transport Interaction in Lithium-Ion Batteries

Lithium-ion batteries have emerged as a key enabler for vehicle electrification and renewable energy integration into the electric grid [43,152,153]. Nanomaterials and nanostructures [43,154–156] in particular have been targeted for electrode development in order to improve the performance (energy and power density), life, and safety of Li-ion batteries. A typical electrode is a composite structure consisting of an electrochemically active intercalation compound, inactive materials, and electrolyte [157,158]. Inactive materials include a conductive additive and a polymeric binder. Polyvinylidene fluoride (PVDF) and carbon black are typical binder and additive materials, respectively. The active material provides lithium storage sites, the binder holds the active material and conductive additive together with the current collector, while the conductive additive enhances the overall electronic conductivity of the composite structure. In this regard, porous electrode microstructures have profound influence on the underlying electrochemical and transport interactions, which ultimately affect the performance, durability, and safety attributes of Li-ion batteries. In this section, we demonstrate, via illustrating examples, the importance of electrode microstructure–transport interplay and the impact on performance, degradation, and safety of Li-ion batteries.

10.1 Illustration of Electrode Microstructure Effect on Performance/Degradation/Safety.

The importance of nanoparticle morphology and assembly on lithium transport and

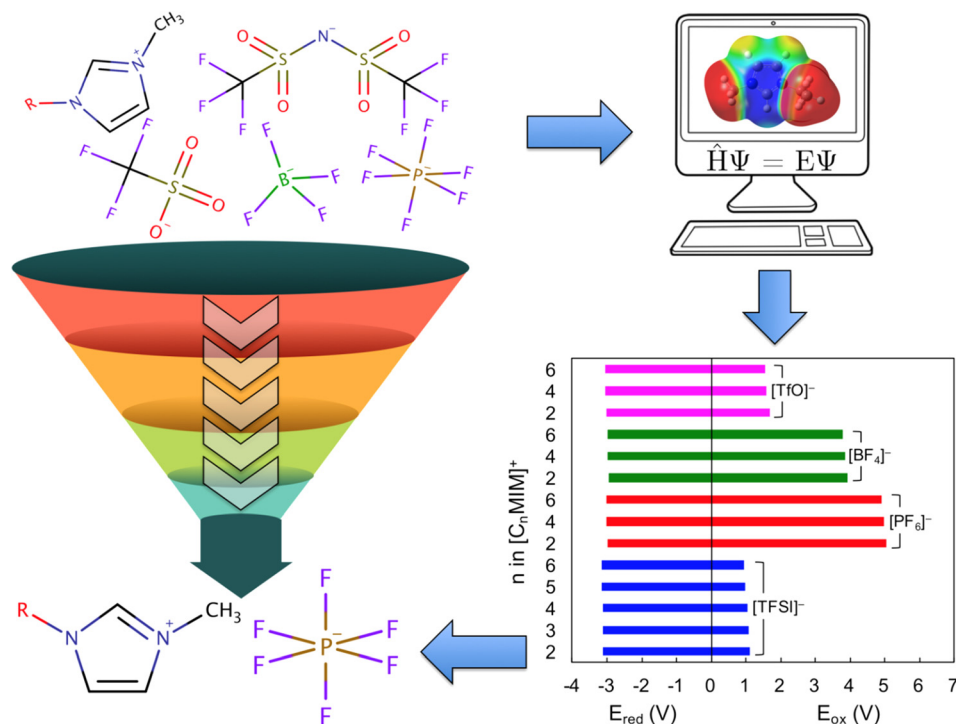


Fig. 12 The schematic, adopted from Banerjee and coworkers [128], depicts atomistic modeling based screening of ionic liquid electrolytes based on their oxidation and reduction potentials

electrochemical performance for the lithium-ion battery cathode has been demonstrated [159]. In this context, it is important to mention that the importance of lithium transport along preferential crystallographic (010) directions has been demonstrated for nanocrystallite LiFePO_4 electrodes [160]. The assembly and columnar stacking of the LiFePO_4 nanocrystallites tend to hinder lithium transport in the active material, with a resultant penalty in the rate capability, as shown in Fig. 13(a) (discharge capacity versus discharge rate) [159]. The shaded area shows pronounced columnar stacking of the nanoplatelets leading to performance deterioration. Figure 13(a) also shows a potential pathway for the mitigation of columnar order via mixing of LiFePO_4 nanoplatelets with isometric additive nanoparticles (labeled as C1 mix).

The secondary phase composition, consisting of the conductive additive and binder, also affects the electrochemical properties and performance of LIBs [79]. Figures 13(b)–13(d) demonstrate the effect of secondary phase composition, with the same electrode porosity, on the cell properties and performance. Figure 13(b) shows that the interfacial area between the active material and the electrolyte increases substantially with the decreasing secondary phase fraction. The active material to secondary phase ratio illustrates a significant impact (shown in Fig. 13(c)) on the pore phase tortuosity which affects the electrolyte transport and also on the effective electronic conductivity. This leads to reduced overpotential and better performance as active material fraction increases. The active material (NMC in this case) has also poor intrinsic electronic conductivity and electron conduction practically results from the conductive additive network, thus with decrease in secondary phase amount, effective electronic conductivity drops appreciably. This negatively affects cell performance at higher rates of operation (see Fig. 13(d)).

Figure 14(a) demonstrates [161] the impact of microstructural variation (e.g., active particle size distribution and electrochemical interface area in this case) on the impedance characteristics,

namely, charge transfer and solid-state diffusion resistances, representative of LIB electrodes, which were stochastically reconstructed. Clearly, the particle size distribution and interfacial area not only affect the charge transfer resistance but also influence the active material network formation, which reflects on the solid-state transport resistance (e.g., slope of the low frequency tail).

Another important inference that can be obtained from the impedance response and capacity fade is that due to the chemomechanical degradation phenomena in the electrodes, such as the SEI formation and microcrack formation in the active particles due to lithium diffusion induced stress. Electrode microstructural attributes play an important role in the chemomechanical degradation aspects [162–164]. For example, a typical graphite electrode with smaller particle size tends to have a larger electrochemically active area which may lead to enhanced SEI formation and hence more profound capacity fade [164]. This is apparent from the simulated electrochemical impedance spectra (EIS) for stochastically reconstructed electrodes with different mean particle sizes after cycling (see Fig. 14(b)). The first semicircle on the EIS spectra corresponds to the evolution of the SEI resistance. The difference in the low frequency tail is attributed to different particle size and equivalently different diffusional resistance. In a nutshell, the electrode microstructure also strongly affects the cell degradation.

Thermal safety due to anomalous temperature excursion locally can be influenced significantly by the electrode microstructural attributes. For example, if the electrode porosity is decreased, it may lead to increased electrolyte transport resistance and subsequently higher Joule heating. Temperature also affects the underlying transport properties. Figure 14(c) representatively demonstrates the influence of electrode microstructures, especially with varying porosity, on the maximum temperature rise and performance based on coupled electrochemical–thermal simulations. The results reveal a nonmonotonic dependence on electrode porosity. Maximum cell temperature

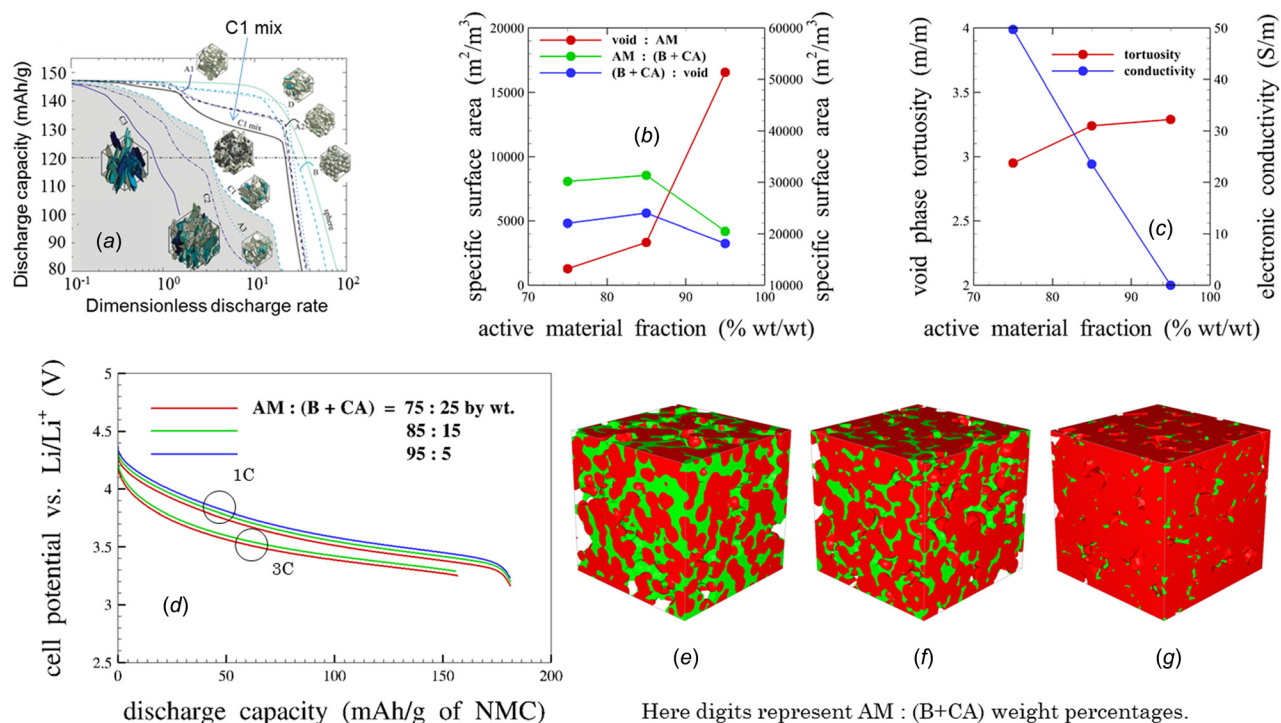


Fig. 13 Illustration of microstructure–performance interplay in typical Li-ion battery electrodes. (a) Effect of packing order of LiFePO_4 on cell performance [159]. (Reproduced with permission from Smith et al. [159]. Copyright 2012 by Royal Society of Chemistry.) The plots (b) and (c) display the variation in microstructural properties as different electrode realization are obtained by keeping the same porosity and different active material weight percentage. Corresponding microstructures are presented in (e) through (g). Subfigure (d) relates the electrochemical performance of $\text{Li}|\text{NMC}$ half cells with these different porous cathode structures. For lower rates of operation ($\leq 1\text{C}$), higher active material leads to better performance but at higher rates (e.g., 3C), higher active material at the expense of conductive additive leads to limitations arising from electron conduction.

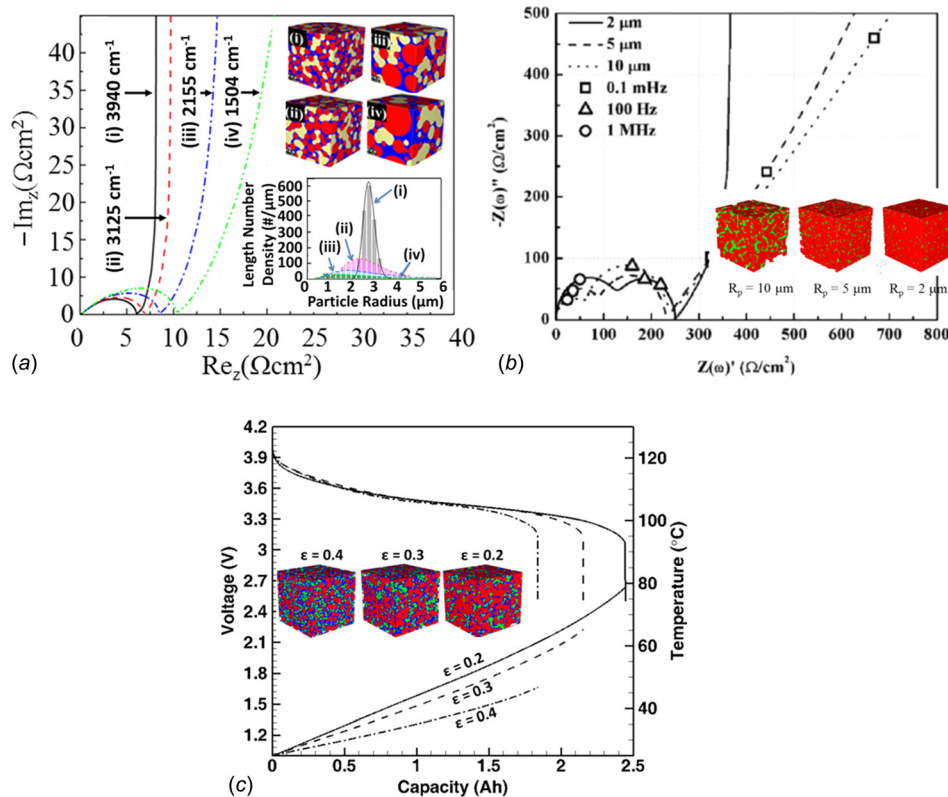


Fig. 14 Effect of typical Li-ion battery electrode microstructures on the impedance and thermal response [161,164]. (a) and (b) Variation in active material mean particle size and size distribution significantly affects the interfacial resistance and impedance response. (c) Electrode porosity plays an important role in electrolyte phase resistance and hence cell temperature rise due to Joule heating. (a) Effect of active material size distribution on EIS (reproduced with permission from Cho et al. [161], copyright 2015 by PCCP, Royal Society of Chemistry), (b) effect of mean particle size on EIS (reproduced with permission from Chen and Mukherjee [164], copyright 2015 by Royal Society of Chemistry), and (c) effect of electrode microstructure on performance and temperature rise.

is related to time integration of heat source terms. This example highlights that by tuning the electrolyte transport resistance via the electrode porosity within a limited window, the internal heat generation and electrochemical utilization can be controlled to achieve cell operation within the safety bounds.

The aforementioned examples, based on a comprehensive set of mesoscale simulations, demonstrate the profound role of electrode microstructures on the performance, degradation, and safety of Li-ion batteries. We would like to proffer the tremendous need for a concerted effort involving physics-based simulations, detailed experiments, and three-dimensional microstructural characteristics to advance the field of electrode science and engineering in lithium-ion battery chemistry and beyond.

11 Conclusion

Based on a recently concluded bilateral workshop on multiphysics phenomena in Li-ion batteries, this paper summarizes the state of the art and future research needs in a wide variety of disciplines relevant to Li-ion batteries. Due to the multiphysics nature of phenomena and processes in Li-ion batteries, a holistic and cross-disciplinary research approach is critical. It is expected that this review article will be useful for researchers in a wide variety of fields relevant to Li-ion batteries.

Acknowledgment

This material is based upon the work supported by the National Science Foundation under Grant Nos. CBET-1623892 and CBET-1554183. P.P.M. and A.M. gratefully acknowledge the financial support from the U.S. Department of Energy (DOE) Computer

Aided Engineering for Batteries (CAEBAT III) program and National Science Foundation (Grant No. 1438431). A.P.C. and W.K.S.C. acknowledge the financial support from the Army Research Office (Award No. W911NF-14-1-0298).

References

- [1] Lascaud, S., Perrier, M., Vallée, A., Besner, S., Prud'homme, J., and Armand, M., 1994, "Phase Diagrams and Conductivity Behavior of Poly(Ethylene Oxide)—Molten Salt Rubbery Electrolytes," *Macromolecules*, **27**(25), pp. 7469–7477.
- [2] Chintapalli, M., Le, T. N. P., Venkatesan, N. R., Mackay, N. G., Rojas, A. A., Thelen, J. L., Chen, X. C., Devaux, D., and Balsara, N. P., 2016, "Structure and Ionic Conductivity of Polystyrene-Block-Poly(Ethylene Oxide) Electrolytes in the High Salt Concentration Limit," *Macromolecules*, **49**(5), pp. 1770–1780.
- [3] Balsara, N. P., Garetz, B. A., and Dai, H. J., 1992, "Relationship Between Birefringence and the Structure of Ordered Block Copolymer Materials," *Macromolecules*, **25**(22), pp. 6072–6074.
- [4] Wang, X., Chintapalli, M., Newstein, M. C., Balsara, N. P., and Garetz, B. A., 2016, "Characterization of a Block Copolymer With a Wide Distribution of Grain Sizes," *Macromolecules*, **49**(21), pp. 8198–8208.
- [5] Pekala, R. W., 1989, "Organic Aerogels From the Polycondensation of Resorcinol With Formaldehyde," *J. Mater. Sci.*, **24**(9), pp. 3221–3227.
- [6] Al-Muhtaseb, S. A., and Ritter, J. A., 2003, "Preparation and Properties of Resorcinol-Formaldehyde Organic and Carbon Gels," *Adv. Mater.*, **15**(2), pp. 101–114.
- [7] Lin, C., and Ritter, J. A., 1997, "Effect of Synthesis pH on the Structure of Carbon Xerogels," *Carbon*, **35**(9), pp. 1271–1278.
- [8] Job, N., Panariello, F., Marien, J., Crine, M., Pirard, J.-P., and Leonard, A., 2006, "Synthesis Optimization of Organic Xerogels Produced From Convective Air-Drying of Resorcinol-Formaldehyde Gels," *J. Non-Cryst. Solids*, **352**(1), pp. 24–34.
- [9] Job, N., Pirard, R., Marien, J., and Pirard, J. P., 2004, "Porous Carbon Xerogels With Texture Tailored by pH Control During Sol-Gel Process," *Carbon*, **42**(3), pp. 619–628.

- [10] Xu, L., Jianwei, L., Jin, D., Yiya, P., and Yitai, Q., 2005, "A Self-Assembly Template Approach to Form Hollow Hexapod-Like, Flower-Like and Tube-Like Carbon Materials," *Carbon*, **43**(7), pp. 1560–1562.
- [11] Shen, J., Li, J., Chen, Q., Luo, T., Yu, W., and Qian, Y., 2006, "Synthesis of Multi-Shell Carbon Microspheres," *Carbon*, **44**(1), pp. 190–193.
- [12] Matos, I., Fernandes, S., Guerreiro, L., Barat, S., Ramos, A. M., Vital, J., and Fonseca, I. M., 2006, "The Effect of Surfactants on the Porosity of Carbon Xerogels," *Microporous Mesoporous Mater.*, **92**, pp. 38–46.
- [13] Sharma, C. S., Kulkarni, M. M., Sharma, A., and Madou, M., 2009, "Synthesis of Carbon Xerogel Particles and Fractal-Like Structures," *Chem. Eng. Sci.*, **64**(7), pp. 1536–1543.
- [14] Sharma, C. S., Upadhyaya, D. K., and Sharma, A., 2009, "Controlling the Morphology of Resorcinol-Formaldehyde Based Carbon Xerogels by Sol Concentration, Shearing and Surfactants," *Ind. Eng. Chem. Res.*, **48**(17), pp. 8030–8036.
- [15] Mezzavilla, S., Zanella, C., Aravind, P. R., Volpe, C. D., and Soraru, G. D., 2012, "Carbon Xerogels as Electrodes for Supercapacitors. The Influence of the Catalyst Concentration on the Microstructure and on the Electrochemical Properties," *J. Mater. Sci.*, **47**(20), pp. 7175–7180.
- [16] Hasegawa, T., Mukai, S. R., Shirato, Y., and Tamon, H., 2004, "Preparation of Carbon Gel Microspheres Containing Silicon Powder for Lithium Ion Battery Anodes," *Carbon*, **42**(12–13), pp. 2573–2579.
- [17] Lee, K. T., Lytle, J. C., Ergang, N. S., Oh, S. M., and Stein, A., 2005, "Synthesis and Rate Performance of Monolithic Macroporous Carbon Electrodes for Lithium-Ion Secondary Batteries," *Adv. Funct. Mater.*, **15**(4), pp. 547–556.
- [18] Sharma, C. S., and Sharma, A., 2015, "Carbon Based Hierarchical Micro- and Nano-Structures: From Synthesis to Applications," *Nanoscale and Microscale Phenomenon: Fundamentals and Applications*, Springer, New Delhi, India.
- [19] Tsuchiya, T., Mori, T., Iwamura, S., Ogino, I., and Mukai, S. R., 2014, "Binder Free Synthesis of High-Surface-Area Carbon Electrodes Via CO₂ Activation of Resorcinol-Formaldehyde Carbon Xerogel Disks: Analysis of Activation Process," *Carbon*, **76**, pp. 240–249.
- [20] Lin, C., and Ritter, J. A., 2000, "Carbonization and Activation of Sol-Gel Derived Carbon Xerogels," *Carbon*, **38**(6), pp. 849–861.
- [21] Awadallah-F, A., and Al-Muhtaseb, S. A., 2012, "Nanofeatures of Resorcinol-Formaldehyde Carbon Microspheres," *Mater. Lett.*, **87**, pp. 31–34.
- [22] Sharma, C. S., Patil, S., Saurabh, S., Sharma, A., and Venkataraghavan, R., 2009, "Resorcinol-Formaldehyde Based Carbon Nanospheres by Electro-spraying," *Bull. Mater. Sci.*, **32**(3), pp. 239–246.
- [23] Mitra, J., Jain, S., Sharma, A., and Basu, B., 2013, "Patterned Growth and Differentiation of Neural Cells on Polymer Derived Carbon Substrates With Micro/Nano Structures In Vitro," *Carbon*, **65**, pp. 140–155.
- [24] Yuan, X., Chao, Y. J., Ma, Z. F., and Deng, X., 2007, "Preparation and Characterization of Carbon Xerogel (CX) and CX-SiO Composite as Anode Material for Lithium-Ion Battery," *Electrochem. Commun.*, **9**(10), pp. 2591–2595.
- [25] Sharma, C. S., Katepalli, H., Sharma, A., Teixidor, G. T., and Madou, M. J., 2014, "Fabrication of Resorcinol-Formaldehyde Xerogel Based High Aspect Ratio 3-D Hierarchical C-MEMS Structures," *ECS Trans.*, **61**(7), pp. 45–54.
- [26] Liu, X., Li, S., Mei, J., Lau, W., Mi, R., Li, Y., Liu, H., and Liu, L., 2014, "From Melamine-Resorcinol-Formaldehyde to Nitrogen-Doped Carbon Xerogels With Micro- and Meso-Pores for Lithium Batteries," *J. Mater. Chem. A*, **2**(35), pp. 14429–14438.
- [27] Kakunuri, M., Vennamala, S., and Sharma, C. S., 2015 "Synthesis of Carbon Xerogel Nanoparticles by Inverse Emulsion Polymerization of Resorcinol-Formaldehyde and Their Use as Anode Materials for Lithium-Ion Battery," *RSC Adv.*, **5**(7), pp. 4747–4753.
- [28] Gopalakrishna, K. M., Kakunuri, M., and Sharma, C. S., 2015, "Effect of Disorder Induced by Ball Milling on the Electrochemical Performance of Catalytically Graphitized," *ECS Trans.*, **66**(8), pp. 41–51.
- [29] Zhang, Z., and Yin, L., 2016 "Polyvinyl Pyrrolidone Wrapped Sn Nanoparticles/Carbon Xerogel Composite as Anode Material for High Performance Lithium Ion Batteries," *Electrochim. Acta*, **212**, pp. 594–602.
- [30] Kakunuri, M., Kali, S., and Sharma, C. S., 2016, "Catalytic Graphitization of Resorcinol-Formaldehyde Xerogel and Its Effect on Lithium Ion Intercalation," *J. Anal. Appl. Pyrolysis*, **117**, pp. 317–324.
- [31] Rey-Raap, N., Piedboeuf, M. C., Arenillas, A., Menéndez, J. A., Léonard, A. F., and Job, N., 2016, "Aqueous and Organic Inks of Carbon Xerogels as Models for Studying the Role of Porosity in Lithium-Ion Battery Electrodes," *Mater. Des.*, **109**, pp. 282–288.
- [32] Piedboeuf, M. C., Léonard, A. F., Deschamps, M., and Job, N., 2016, "Carbon Xerogels as Model Materials: Toward a Relationship Between Pore Texture and Electrochemical Behavior as Anodes for Lithium-Ion Batteries," *J. Mater. Sci.*, **51**(9), pp. 4358–4370.
- [33] Lahiri, I., Oh, S.-W., Hwang, J. Y., Cho, S., Sun, Y.-K., Banerjee, R., and Choi, W., 2010, "High Capacity and Excellent Stability of Lithium Ion Battery Using Interface-Controlled Binder-Free Multiwall Carbon Nanotubes Grown on Copper," *ACS Nano*, **4**(6), pp. 3440–3446.
- [34] Lahiri, I., Oh, S.-M., Hwang, J. Y., Kang, C., Choi, M., Jeon, H., Banerjee, R., Sun, Y.-K., and Choi, W., 2011, "Ulathin Alumina-Coated Carbon Nanotubes as an Anode for High Capacity Li-Ion Batteries," *J. Mater. Chem.*, **21**(35), pp. 13621–13626.
- [35] Lahiri, I., Lahiri, D., Jin, S., Agarwal, A., and Choi, W., 2011, "Carbon Nanotubes: How Strong Is Their Bonding With the Substrate?," *ACS Nano*, **5**(2), pp. 780–787.
- [36] Tahil, W., 2010, "How Much Lithium Does a Lilon EV Battery Really Need?," Meridian International Research, Martainville, France, accessed Apr. 26, 2017, http://www.meridian-int-res.com/Projects/How_Much_Lithium_Per_Battery.pdf
- [37] Evanoff, K., Khan, J., Balandin, A. A., Magasinski, A., Ready, W. J., Fuller, T. F., and Yushin, G., 2012, "Towards Ultrathick Battery Electrodes: Aligned Carbon Nanotube-Enabled Architecture," *Adv. Mater.*, **24**(4), pp. 533–537.
- [38] Gohier, A., Laik, B., Kim, K.-H., Maurice, J.-L., Pereira-Ramos, J.-P., Cojocaru, C. S., and Van, P. T., 2012, "High-Rate Capability Silicon Decorated Vertically Aligned Carbon Nanotubes for Li-Ion Batteries," *Adv. Mater.*, **24**(19), pp. 2592–2597.
- [39] Shaijumon, M. M., Perre, E., Daffos, B., Taberna, P. L., Tarascon, J.-M., and Simon, P., 2010, "Nanoarchitected 3D Cathodes for Li-Ion Microbatteries," *Adv. Mater.*, **22**(44), pp. 4978–4981.
- [40] Ripenbein, T., Golodnitsky, D., Nathan, M., and Peled, E., 2010, "Novel Porous-Silicon Structures for 3D-Interlaced Microbatteries," *Electrochim. Acta*, **56**(1), pp. 37–41.
- [41] Kang, C., Lahiri, I., Baskaran, R., Kim, W.-G., Sun, Y.-K., and Choi, W., 2012, "3-Dimensional Carbon Nanotube for Li-Ion Battery Anode," *J. Power Sources*, **219**, pp. 364–370.
- [42] USCAR, 2006, "USABC Goals for Advanced Batteries for EVs—CY 2020 Commercialization," United States Council for Automotive Research LLC, Southfield, MI, accessed Apr. 26, 2017, http://uscar.org/guest/article_view.php?articles_id=85
- [43] Goodenough, J. B., and Park, K.-S., 2013, "The Li-Ion Rechargeable Battery: A Perspective," *J. Am. Chem. Soc.*, **135**(4), pp. 1167–1176.
- [44] Thackeray, M. M., Wolverton, C., and Isaacs, E. D., 2012, "Electrical Energy Storage for Transportation—Approaching the Limits of, and Going Beyond, Lithium-Ion Batteries," *Energy Environ. Sci.*, **5**(7), pp. 7854–7863.
- [45] Thackeray, M. M., Kang, S.-H., Johnson, C. S., Vaughey, J. T., Benedek, R., and Hackney, S. A., 2007, "Li₂MnO₃-Stabilized LiMO₂ (M = Mn, Ni, Co) Electrodes for Lithium-Ion Batteries," *Mater. Chem.*, **17**(30), pp. 3112–3125.
- [46] Armstrong, A. R., Holzapfel, M., Novák, P., Johnson, C. S., Kang, S.-H., Thackeray, M. M., and Bruce, P. G., 2006, "Demonstrating Oxygen Loss and Associated Structural Reorganization in the Lithium Battery Cathode Li[Ni_{0.2}Li_{0.2}Mn_{0.6}O₂]," *J. Am. Chem. Soc.*, **128**(26), pp. 8694–8698.
- [47] Martha, S. K., Nanda, J., Veith, G. M., and Dudney, N. J., 2012, "Electrochemical and Rate Performance Study of High-Voltage Lithium-Rich Composition: Li_{1.2}Mn_{0.525}Ni_{0.175}Co_{0.1}O₂," *J. Power Sources*, **199**, pp. 220–226.
- [48] Martha, S. K., Nanda, J., Veith, G. M., and Dudney, N. J., 2012, "Surface Cycles of High Voltage Lithium Rich Composition: Li_{1.2}Mn_{0.525} Ni_{0.175} Co_{0.1}O₂," *J. Power Sources*, **216**, pp. 179–186.
- [49] Martha, S. K., Nanda, J., Kim, Y., Unocic, R., Pannala, S., and Dudney, N. J., 2013, "Solid Electrolyte Coated High Voltage Layered-Layered Lithium-Rich Composite Cathode: Li_{1.2}Mn_{0.525}Ni_{0.175}Co_{0.1}O₂," *J. Mater. Chem. A*, **1**(18), pp. 5587–5595.
- [50] Yang, F., Liu, Y., Martha, S. K., Wu, Z., Andrews, J. C., Ice, G. E., Pianetta, P., and Nanda, J., 2014, "Nanoscale Morphological and Chemical Changes of High Voltage Lithium-Manganese Rich NMC Composite Cathodes With Cycling," *Nano Lett.*, **14**(8), pp. 4334–4341.
- [51] Wu, Y., Murugan, A. V., and Manthiram, A., 2008, "Surface Modification of High Capacity Layered Li [Li_{0.2}Mn_{0.54}Ni_{0.13}Co_{0.13}]O₂ Cathodes by AlPO₄," *J. Electrochem. Soc.*, **155**(9), pp. A635–A641.
- [52] Mohanty, D., Dahlberg, K., King, D. M., David, L. A., Sefat, A. S., Wood, D. L., Daniel, C., Dhar, S., Mahajan, V., Lee, M., and Albano, F., 2016, "Modification of Ni-Rich FCG NMC and NCA Cathodes by Atomic Layer Deposition: Preventing Surface Phase Transitions for High-Voltage Lithium-Ion Batteries," *Sci. Rep.*, **6**, pp. 1–16.
- [53] Bettge, M., Li, Y., Sankaran, B., Rago, N. D., Spila, T., Haasch, R. T., Petrov, I., and Abraham, D. P., 2013, "Improving High-Capacity Li_{1.2}Ni_{0.15}Mn_{0.55}Co_{0.1}O₂-Based Lithium-Ion Cells by Modifying the Positive Electrode With Alumina," *J. Power Sources*, **233**, pp. 346–357.
- [54] Croguennec, L., Bains, J., Ménétrier, M., Flambard, A., Bekaert, E., Jordy, C., Biensan, P., and Delmas, C., 2009, "Synthesis of 'Li_{1.1}(Ni_{0.425}Mn_{0.425}Co_{0.15})O₂F_{0.2}' Materials by Different Routes: Is There Fluorine Substitution, for Oxygen?," *J. Electrochem. Soc.*, **156**(5), pp. A349–A355.
- [55] Satishkumar, B. C., Bernadi, D. M., and Liu, L., 2014, "A Review of Blended Cathode Materials for Use in Li-Ion Batteries," *J. Power Sources*, **248**, pp. 91–100.
- [56] Oh, S. W., Park, S. H., Kim, J. H., Bae, Y. H., and Sun, Y. K., 2006, "Improvement of Electrochemical Properties of LiNi_{0.5}Mn_{1.5}O₄ Spinel Material by Fluorine Substitution," *J. Power Sources*, **157**(1), pp. 464–470.
- [57] Cocco, A. P., Nelson, G. J., Harris, W. M., Nakajo, A., Myles, T. D., Kiss, A. M., Lombardo, J. J., and Chiu, W. K., 2013, "Three-Dimensional Microstructural Imaging Methods for Energy Materials," *Phys. Chem. Chem. Phys.*, **15**(39), pp. 16377–16407.
- [58] Shearing, P. R., Howard, L. E., Jørgensen, P. S., Brandon, N. P., and Harris, S. J., 2010, "Characterization of the 3-Dimensional Microstructure of a Graphite Negative Electrode From a Li-Ion Battery," *Electrochem. Commun.*, **12**(3), pp. 374–377.
- [59] Lupis, C. H., 1983, *Chemical Thermodynamics of Materials*, Elsevier, New York, p. 581.
- [60] Ratke, L., and Voorhees, P. W., 2002, *Growth and Coarsening: Ripening in Materials Processing*, Springer, Berlin.
- [61] Thiedmann, R., Stenzel, O., Spettl, A., Shearing, P. R., Harris, S. J., Brandon, N. P., and Schmidt, V., 2011, "Stochastic Simulation Model for the 3D Morphology of Composite Materials in Li-Ion Batteries," *Comput. Mater. Sci.*, **50**(12), pp. 3365–3376.
- [62] Nelson, G. J., van Zandt, Z. K., and Jibhakate, P. D., 2016, "Direct X-Ray Imaging as a Tool for Understanding Multiphysics Phenomena in Energy Storage," *ASME J. Electrochem. Energy Convers. Storage*, **13**(3), p. 030802.

- [63] Roberts, S. A., Mendoza, H., Brunini, V. E., Trembacki, B. L., Noble, D. R., and Grillet, A. M., 2016, "Insights Into Lithium-Ion Battery Degradation and Safety Mechanisms From Mesoscale Simulations Using Experimentally Reconstructed Mesoscale Structures," *ASME J. Electrochem. Energy Convers. Storage*, **13**(3), p. 031005.
- [64] Grew, K. N., Chu, Y. S., Yi, J., Peracchio, A. A., Izzo, J. R., Hwu, Y., De Carlo, F., and Chiu, W. K., 2010, "Nondestructive Nanoscale 3D Elemental Mapping and Analysis of a Solid Oxide Fuel Cell Anode," *J. Electrochem. Soc.*, **157**(6), pp. B783–B792.
- [65] Harris, W. M., Nelson, G. J., Kiss, A. M., Izzo, J. R., Liu, Y., Liu, M., Wang, S., Chu, Y. S., and Chiu, W. K., 2012, "Nondestructive Volumetric 3-D Chemical Mapping of Nickel-Sulfur Compounds at the Nanoscale," *Nanoscale*, **4**(5), pp. 1557–1560.
- [66] Harris, W. M., and Chiu, W. K., 2015, "Determining the Representative Volume Element Size for Three-Dimensional Microstructural Material Characterization—Part 1: Predictive Models," *J. Power Sources*, **282**, pp. 552–561.
- [67] Harris, W. M., and Chiu, W. K., 2015, "Determining the Representative Volume Element Size for Three-Dimensional Microstructural Material Characterization—Part 2: Application to Experimental Data," *J. Power Sources*, **282**, pp. 622–629.
- [68] Grew, K. N., Peracchio, A. A., and Chiu, W. K., 2010, "Characterization and Analysis Methods for the Examination of the Heterogeneous Solid Oxide Fuel Cell Electrode Microstructure—Part 2: Quantitative Measurement of the Microstructure and Contributions to Transport Losses," *J. Power Sources*, **195**(24), pp. 7943–7958.
- [69] Grew, K. N., Peracchio, A. A., Joshi, A. S., Izzo, J. R., and Chiu, W. K., 2010, "Characterization and Analysis Methods for the Examination of the Heterogeneous Solid Oxide Fuel Cell Electrode Microstructure—Part 1: Volumetric Measurements of the Heterogeneous Structure," *J. Power Sources*, **195**(24), pp. 7930–7942.
- [70] Nelson, G. J., Harris, W. M., Izzo, J. R., Jr., Grew, K. N., Chiu, W. K., Chu, Y. S., Yi, J., Andrews, J. C., Liu, Y., and Pianetta, P., 2011, "Three-Dimensional Mapping of Nickel Oxidation States Using Full Field X-Ray Absorption Near Edge Structure Nanotomography," *Appl. Phys. Lett.*, **98**(17), p. 173109.
- [71] Izzo, J. R., Joshi, A. S., Grew, K. N., Chiu, W. K., Tkachuk, A., Wang, S. H., and Yun, W., 2008, "Nondestructive Reconstruction and Analysis of SOFC Anodes Using X-Ray Computed Tomography at Sub-50 nm Resolution," *J. Electrochem. Soc.*, **155**(5), pp. B504–B508.
- [72] Joshi, A. S., Grew, K. N., Izzo, J. R., Peracchio, A. A., and Chiu, W. K., 2010, "Lattice Boltzmann Modeling of Three-Dimensional, Multicomponent Mass Diffusion in a Solid Oxide Fuel Cell Anode," *ASME J. Fuel Cell Sci. Technol.*, **7**(1), p. 011006.
- [73] Mendoza, R., Savin, I., Thornton, K., and Voorhees, P. W., 2004, "Topological Complexity and the Dynamics of Coarsening," *Nat. Mater.*, **3**(6), pp. 385–388.
- [74] Glicksman, M. E., and Voorhees, P. W., 1984, "Ostwald Ripening and Relaxation in Dendritic Structures," *Metall. Trans. A*, **15**(6), pp. 995–1001.
- [75] Alkemper, J., and Voorhees, P. W., 2001, "Three-Dimensional Characterization of Dendritic Microstructures," *Acta Mater.*, **49**(5), pp. 897–902.
- [76] Kammer, D., and Voorhees, P. W., 2006, "The Morphological Evolution of Dendritic Microstructures During Coarsening," *Acta Mater.*, **54**(6), pp. 1549–1558.
- [77] FEI, 2012, "Avizo 7 Reference Guide," FEI, Hillsboro, OR, accessed Apr. 26, 2017, <https://www.fei.com/software/avizo-user-guide/>
- [78] Jithin, M., Das, M. K., and De, A., 2016, "Lattice Boltzmann Simulation of Lithium Peroxide Formation in Lithium–Oxygen Battery," *ASME J. Electrochem. Energy Convers. Storage*, **13**(3), p. 031003.
- [79] Mistry, A., Juarez-Robles, D., Stein, M., Smith, K., and Mukherjee, P. P., 2016, "Analysis of Long-Range Interaction in Lithium-Ion Battery Electrodes," *ASME J. Electrochem. Energy Convers. Storage*, **13**(3), p. 031006.
- [80] Shah, K., Vishwakarma, V., and Jain, A., 2016, "Measurement of Multiscale Thermal Transport Phenomena in Li-Ion Cells: A Review," *ASME J. Electrochem. Energy Convers. Storage*, **13**(3), p. 030801.
- [81] McGaughey, A. J. H., and Kaviany, M., 2006, "Phonon Transport in Molecular Dynamics Simulations: Formulation and Thermal Conductivity Prediction," *Adv. Heat Transfer*, **39**, pp. 169–255.
- [82] Hegedus, P. J., and Abramson, A. R., 2006, "A Molecular Dynamics Study of Interfacial Thermal Transport in Heterogeneous Systems," *Int. J. Heat Mass Transfer*, **49**, pp. 4921–4931.
- [83] Tien, C.-L., Lukes, J. R., and Chou, F.-C., 1998, "Molecular Dynamics Simulation of Thermal Transport in Solids," *Microscale Thermophys. Eng.*, **2**(3), pp. 133–137.
- [84] Vishwakarma, V., Waghela, C., Wei, Z., Prasher, R., Nagpure, S. C., Li, J., Liu, F., Daniel, C., and Jain, A., 2015, "Heat Transfer Enhancement in a Lithium-Ion Cell Through Improved Material-Level Thermal Transport," *J. Power Sources*, **300**, pp. 123–131.
- [85] Ye, Y., Saw, L. H., Shi, Y., Somasundaram, K., and Tay, A. A., 2014, "Effect of Thermal Contact Resistances on Fast Charging of Large Format Lithium Ion Batteries," *Electrochim. Acta*, **134**, pp. 327–337.
- [86] Shah, K., Drake, S. J., Wetz, D. A., Ostanek, J. K., Miller, S. P., Heinzl, J. M., and Jain, A., 2014, "Modeling of Steady-State Convective Cooling of Cylindrical Li-Ion Cells," *J. Power Sources*, **258**, pp. 374–381.
- [87] Shah, K., Drake, S. J., Wetz, D. A., Ostanek, J. K., Miller, S. P., Heinzl, J. M., and Jain, A., 2014, "An Experimentally Validated Transient Thermal Model for Cylindrical Li-Ion Cells," *J. Power Sources*, **271**, pp. 262–268.
- [88] Lopez, C. F., Jeevarajan, J. A., and Mukherjee, P. P., 2016, "Evaluation of Combined Active and Passive Thermal Management Strategies for Lithium-Ion Batteries," *ASME J. Electrochem. Energy Convers. Storage*, **13**(3), p. 031007.
- [89] Ramadesigan, V., Northrop, P. W. C., De, S., Santhanagopalan, S., Braatz, R. D., and Subramanian, V. R., 2012, "Modeling and Simulation of Lithium-Ion Batteries From a Systems Engineering Perspective," *J. Electrochem. Soc.*, **159**(3), pp. R31–R45.
- [90] Doyle, M., Fuller, T. F., and Newman, J., 1993, "Modeling of Galvanostatic Charge and Discharge of the Lithium/Polymer/Insertion Cell," *J. Electrochem. Soc.*, **140**(6), pp. 1526–1533.
- [91] Botte, G. G., Subramanian, V. R., and White, R. E., 2000, "Mathematical Modeling of Secondary Lithium Batteries," *Electrochim. Acta*, **45**(15–16), pp. 2595–2609.
- [92] Torchio, M., Magni, L., Gopaluni, R. B., Braatz, R. D., and Raimondo, D. M., 2016, "LIONSIMBA: A Matlab Framework Based on a Finite Volume Model Suitable for Li-Ion Battery Design, Simulation, and Control," *J. Electrochem. Soc.*, **163**(7), pp. A1192–A1205.
- [93] Subramanian, V. R., Boovaragavan, V., Ramadesigan, V., and Arabandi, M., 2009, "Mathematical Model Reformulation for Lithium-Ion Battery Simulations: Galvanostatic Boundary Conditions," *J. Electrochem. Soc.*, **156**(4), pp. A260–A271.
- [94] Cai, L., and White, R. E., 2012, "Lithium Ion Cell Modeling Using Orthogonal Collocation on Finite Elements," *J. Power Sources*, **217**, pp. 248–255.
- [95] Northrop, P. W. C., Ramadesigan, V., De, S., and Subramanian, V. R., 2011, "Coordinate Transformation, Orthogonal Collocation, Model Reformulation and Simulation of Electrochemical-Thermal Behavior of Lithium-Ion Battery Stacks," *J. Electrochem. Soc.*, **158**(12), pp. A1461–A1477.
- [96] Zhang, Q., and White, R. E., 2007, "Comparison of Approximate Solution Methods for the Solid Phase Diffusion Equation in a Porous Electrode Model," *J. Power Sources*, **165**(2), pp. 880–886.
- [97] Ramadesigan, V., Boovaragavan, V., Pirkle, J. C., and Subramanian, V. R., 2010, "Efficient Reformulation of Solid-Phase Diffusion in Physics-Based Lithium-Ion Battery Models," *J. Electrochem. Soc.*, **157**(7), pp. A854–A860.
- [98] Jagannathan, K., 2009, "Approximate Solution Methods for Solid-State Diffusion in Phase-Change Electrodes," *J. Electrochem. Soc.*, **156**(12), pp. A1028–A1033.
- [99] Subramanian, V. R., Diwakar, V. D., and Tapriyal, D., 2005, "Efficient Macro-Micro Scale Coupled Modeling of Batteries," *J. Electrochem. Soc.*, **152**(10), pp. A2002–A2008.
- [100] Northrop, P. W. C., Suthar, B., Ramadesigan, V., Santhanagopalan, S., Braatz, R. D., and Subramanian, V. R., 2014, "Efficient Simulation and Reformulation of Lithium-Ion Battery Models for Enabling Electric Transportation," *J. Electrochem. Soc.*, **161**(8), pp. E3149–E3157.
- [101] MathWorks, 2017, "ode45 (Matlab)," The MathWorks, Inc., Natick, MA, accessed Sept. 20, 2016, <https://www.mathworks.com/help/matlab/ref/ode45.html>
- [102] Hairer, E., and Wanner, G., 1996, *Solving Ordinary Differential Equations: II—Stiff and Differential-Algebraic Problems*, Springer, Berlin.
- [103] Hairer, E., and Wanner, G., 2010, "Linear Multistep Methods," *Scholarpedia*, **5**(4), p. 4591.
- [104] Brenan, K., Campbell, S., and Petzold, L., 1995, *Numerical Solution of Initial-Value Problems in Differential-Algebraic Equations*, Society for Industrial and Applied Mathematics, Philadelphia, PA.
- [105] Van Keken, P. E., Yuen, D. A., and Petzold, L. R., 1995, "DASPK: A New High Order and Adaptive Time-Integration Technique With Applications to Mantle Convection With Strongly Temperature- and Pressure-Dependent Rheology," *Geophys. Astrophys. Fluid Dyn.*, **80**(1–2), pp. 57–74.
- [106] Hindmarsh, A. C., Brown, P. N., Grant, K. E., Lee, S. L., Serban, R., Shumaker, D. E., and Woodward, C. S., 2005, "SUNDIALS: Suite of Nonlinear and Differential/Algebraic Equation Solvers," *ACM Trans. Math. Software*, **31**(3), pp. 363–396.
- [107] Alexander, R., 1977, "Diagonally Implicit Runge–Kutta Methods for Stiff O.D.E.'s," *SIAM J. Numer. Anal.*, **14**(6), pp. 1006–1021.
- [108] Cash, J. R., and Considine, S., 1992, "An MEBDF Code for Stiff Initial Value Problems," *ACM Trans. Math. Software*, **18**(2), pp. 142–155.
- [109] Cash, J. R., and Singhal, A., 1982, "Mono-Implicit Runge–Kutta Formulae for the Numerical Integration of Stiff Differential Systems," *IMA J. Numer. Anal.*, **2**(2), pp. 211–227.
- [110] Wu, B., and White, R. E., 2001, "An Initialization Subroutine for DAEs Solvers: DAEIS," *Comput. Chem. Eng.*, **25**(2–3), pp. 301–311.
- [111] Methekar, R. N., Ramadesigan, V., Pirkle, J. C., Subramanian, V. R., Pirkle, J. C., Jr., Subramanian, V. R., Pirkle, J. C., and Subramanian, V. R., 2011, "A Perturbation Approach for Consistent Initialization of Index-1 Explicit Differential–Algebraic Equations Arising From Battery Model Simulations," *Comput. Chem. Eng.*, **35**(11), pp. 2227–2234.
- [112] Lawder, M. T., Ramadesigan, V., Suthar, B., and Subramanian, V. R., 2015, "Extending Explicit and Linearly Implicit ODE Solvers for Index-1 DAEs," *Comput. Chem. Eng.*, **82**, pp. 283–292.
- [113] Bruce, P. G., Freunberger, S. A., Hardwick, L. J., and Tarascon, J. M., 2011, "Li-O₂ and Li-S Batteries With High Energy Storage," *Nat. Mater.*, **11**(1), pp. 19–29.
- [114] Girishkumar, G., McCloskey, B., Luntz, A. C., Swanson, S., and Wilcke, W., 2010, "Lithium–Air Battery: Promise and Challenges," *J. Phys. Chem. Lett.*, **1**(14), pp. 2193–2203.
- [115] Jung, Y., and Kim, S., 2007, "New Approaches to Improve Cycle Life Characteristics of Lithium–Sulfur Cells," *Electrochem. Commun.*, **9**(2), pp. 249–254.
- [116] Xiao, L., Cao, Y., Xiao, J., Schwenzer, B., Engelhard, M. H., Saraf, L. V., Nie, Z., Exarhos, G. J., and Liu, J., 2012, "A Soft Approach to Encapsulate

- Sulfur: Polyaniline Nanotubes for Lithium-Sulfur Batteries With Long Cycle Life," *Adv. Mater.*, **24**(9), pp. 1176–1181.
- [117] Jayaprakash, N., Shen, J., Moganty, S. S., Corona, A., and Archer, L. A., 2011, "Porous Hollow Carbon@Sulfur Composites for High-Power Lithium-Sulfur Batteries," *Angew. Chem.*, **123**(26), pp. 6026–6030.
- [118] Feng, X., Song, M. K., Stolte, W. C., Gardenghi, D., Zhang, D., Sun, X., Zhu, J., Cairns, E. J., and Guo, J., 2014, "Understanding the Degradation Mechanism of Rechargeable Lithium/Sulfur Cells: A Comprehensive Study of the Sulfur-Graphene Oxide Cathode After Discharge-Charge Cycling," *Phys. Chem. Chem. Phys.*, **16**(32), pp. 16931–16940.
- [119] Li, N., Zheng, M., Lu, H., Hu, Z., Shen, C., Chang, X., Ji, G., Cao, J., and Shi, Y., 2012, "High-Rate Lithium-Sulfur Batteries Promoted by Reduced Graphene Oxide Coating," *Chem. Commun.*, **48**(34), pp. 4106–4108.
- [120] Sun, K., Liu, H., and Gan, H., 2016, "Cathode Loading Effect on Sulfur Utilization in Lithium-Sulfur Battery," *ASME J. Electrochem. Energy Convers. Storage*, **13**(2), p. 021002.
- [121] Guan, D., and Yuan, C., 2016, "Enhancing the Cycling Stability of Tin Sulfide Anodes for Lithium Ion Battery by Titanium Oxide Atomic Layer Deposition," *ASME J. Electrochem. Energy Convers. Storage*, **13**(2), p. 021004.
- [122] Tan, S., Ji, Y. J., Zhang, Z. R., and Yang, Y., 2014, "Recent Progress in Research on High-Voltage Electrolytes for Lithium-Ion Batteries," *ChemPhysChem*, **15**(10), pp. 1956–1969.
- [123] Ramos-Sanchez, G., Soto, F. A., de la Hoz, J. M., Liu, Z., Mukherjee, P. P., El-Mellouhi, F., Seminario, J. M., and Balbuena, P. B., 2016, "Computational Studies of Interfacial Reactions at Anode Materials: Initial Stages of the Solid-Electrolyte-Interphase Layer Formation," *ASME J. Electrochem. Energy Convers. Storage*, **13**(3), p. 031002.
- [124] Nicotera, L., Oliviero, C., Henderson, W. A., Appetecchi, G. B., and Passerini, S., 2005, "NMR Investigation of Ionic Liquid-LiX Mixtures: Pyrrolidinium Cations and TFSI-Anions," *J. Phys. Chem. B*, **109**(48), pp. 22814–22819.
- [125] Kim, G. T., Jeong, S. S., Xue, M. Z., Balducci, A., Winter, M., Passerini, S., Alessandrini, F., and Appetecchi, G. B., 2012, "Development of Ionic Liquid-Based Lithium Battery Prototypes," *J. Power Sources*, **199**, pp. 239–246.
- [126] Tokuda, H., Hayamizu, K., Ishii, K., Abu Bin Hasan Susan, M., and Watanabe, M., 2004, "Physicochemical Properties and Structures of Room Temperature Ionic Liquids—I: Variation of Anionic Species," *J. Phys. Chem. B*, **108**(42), pp. 16593–16600.
- [127] Galinski, M., Lewandowski, A., and Stepniak, I., 2006, "Ionic Liquids as Electrolytes," *Electrochim. Acta*, **51**(26), pp. 5567–5580.
- [128] Kazemiabnavi, S., Zhang, Z., Thornton, K., and Banerjee, S., 2016, "Electrochemical Stability Window of Imidazolium-Based Ionic Liquids as Electrolytes for Lithium Batteries," *J. Phys. Chem. B*, **120**(25), pp. 5691–5702.
- [129] Borodin, O., and Smith, G. D., 2006, "Structure and Dynamics of N-Methyl-N-Propylpyrrolidinium bis(Trifluoromethanesulfonyl)Imide Ionic Liquid From Molecular Dynamics Simulations," *J. Phys. Chem. B*, **110**(23), pp. 11481–11490.
- [130] Bayley, P. M., Lane, G. H., Rocher, N. M., Clare, B. R., Best, A. S., MacFarlane, D. R., and Forsyth, M., 2009, "Transport Properties of Ionic Liquid Electrolytes With Organic Diluents," *Phys. Chem. Chem. Phys.*, **11**(33), pp. 7202–7208.
- [131] Raju, S. G., and Balasubramanian, S., 2010, "Molecular Dynamics Simulation of Model Room Temperature Ionic Liquids With Divalent Anions," *Indian J. Chem. Sect. A*, **49**(5–6), pp. 721–726.
- [132] Bayley, P. M., Best, A. S., MacFarlane, D. R., and Forsyth, M., 2011, "The Effect of Coordinating and Non-Coordinating Additives on the Transport Properties in Ionic Liquid Electrolytes for Lithium Batteries," *Phys. Chem. Chem. Phys.*, **13**(10), pp. 4632–4640.
- [133] Seki, S., Kobayashi, Y., Miyashiro, H., Ohno, Y., Usami, A., Mita, Y., Kihira, N., Watanabe, M., and Terada, N., 2006, "Lithium Secondary Batteries Using Modified-Imidazolium Room-Temperature Ionic Liquid," *J. Phys. Chem. B*, **110**(21), pp. 10228–10230.
- [134] Lane, G. H., Best, A. S., MacFarlane, D. R., Forsyth, M., Bayley, P. M., and Hollenkamp, A. F., 2010, "The Electrochemistry of Lithium in Ionic Liquid/Organic Diluent Mixtures," *Electrochim. Acta*, **55**(28), pp. 8947–8952.
- [135] Hardwick, L. J., Holzapfel, M., Wokaun, A., and Novak, P., 2007, "Raman Study of Lithium Coordination in EMI-TFSI Additive Systems as Lithium-Ion Battery Ionic Liquid Electrolytes," *J. Raman Spectrosc.*, **38**(1), pp. 110–112.
- [136] Xu, J. Q., Yang, J., NuLi, Y., Wang, J. L., and Zhang, Z. S., 2006, "Additive-Containing Ionic Liquid Electrolytes for Secondary Lithium Battery," *J. Power Sources*, **160**(1), pp. 621–626.
- [137] Choi, J. A., Eo, S. M., MacFarlane, D. R., Forsyth, M., Cha, E., and Kim, D. W., 2008, "Effect of Organic Additives on the Cycling Performances of Lithium Metal Polymer Cells," *J. Power Sources*, **178**(2), pp. 832–836.
- [138] Deshpande, A., Kariyawasam, L., Dutta, P., and Banerjee, S., 2013, "Enhancement of Lithium Ion Mobility in Ionic Liquid Electrolytes in Presence of Additives," *J. Phys. Chem. C*, **117**(48), pp. 25343–25351.
- [139] Newman, J. S., and Thomas-Alyea, K. E., 2004, *Electrochemical Systems*, 3rd ed., Wiley-Interscience, Hoboken, NJ.
- [140] Yoo, K., Banerjee, S., and Dutta, P., 2014, "Modeling of Volume Change Phenomena in a Li-Air Battery," *J. Power Sources*, **258**, pp. 340–350.
- [141] Yoo, K., Deshpande, A., Banerjee, S., and Dutta, P., 2015, "Electrochemical Model for Ionic Liquid Electrolytes in Lithium Batteries," *Electrochim. Acta*, **176**, pp. 301–310.
- [142] Hummelshøj, J. S., Blomqvist, J., Datta, S., Vegge, T., Rossmeisl, J., Thygesen, K. S., Luntz, A. C., Jacobsen, K. W., and Nørskov, J. K., 2010, "Communications: Elementary Oxygen Electrode Reactions in the Aprotic Li-Air Battery," *J. Chem. Phys.*, **132**(7), p. 071101.
- [143] Kazemiabnavi, S., Dutta, P., and Banerjee, S., 2014, "Ab Initio Modeling of the Electron Transfer Reaction Rate at the Electrode-Electrolyte Interface in Lithium-Air Batteries," *ASME Paper No. IMECE2014-40239*.
- [144] Kazemiabnavi, S., Dutta, P., and Banerjee, S., 2014, "Density Functional Theory Based Study of the Electron Transfer Reaction at the Lithium Metal Anode in a Lithium-Air Battery With Ionic Liquid Electrolytes," *J. Phys. Chem. C*, **118**(47), pp. 27183–27192.
- [145] Truhlar, D. G., Garrett, B. C., and Klippenstein, S. J., 1996, "Current Status of Transition-State Theory," *J. Phys. Chem.*, **100**(31), pp. 12771–12800.
- [146] Truhlar, D. G., and Garrett, B. C., 1984, "Variational Transition State Theory," *Annu. Rev. Phys. Chem.*, **35**(1), pp. 159–189.
- [147] Wang, Y., Qian, Y., Feng, W. L., and Liu, R. Z., 2003, "Implementation of a Microcanonical Variational Transition State Theory for Direct Dynamics Calculations of Rate Constants," *Sci. China Ser. B*, **46**(3), pp. 225–233.
- [148] Garrett, B. C., and Truhlar, D. G., 1979, "Generalized Transition State Theory. Canonical Variational Calculations Using the Bond Energy-Bond Order Method for Bimolecular Reactions of Combustion Products," *J. Am. Chem. Soc.*, **101**(18), pp. 5207–5217.
- [149] Marcus, R. A., 1997, "Electron Transfer Reactions in Chemistry Theory and Experiment," *Pure Appl. Chem.*, **69**(1), pp. 13–29.
- [150] Kowalczyk, T., Wang, L.-P., and Van Voorhis, T., 2011, "Simulation of Solution Phase Electron Transfer in a Compact Donor-Acceptor Dyad," *J. Phys. Chem. B*, **115**(42), pp. 12135–12144.
- [151] Kazemiabnavi, S., Dutta, P., and Banerjee, S., 2015, "A Density Functional Theory Based Study of the Electron Transfer Reaction at the Cathode-Electrolyte Interface in Lithium-Air Batteries," *Phys. Chem. Chem. Phys.*, **17**(17), pp. 11740–11751.
- [152] Armand, M., and Tarascon, J. M., 2008, "Building Better Batteries," *Nature*, **451**(7179), pp. 652–657.
- [153] Dunn, B., Kamath, H., and Tarascon, J. M., 2011, "Electrical Energy Storage for the Grid: A Battery of Choices," *Science*, **334**(6058), pp. 928–935.
- [154] Obrovac, M. N., and Chevrier, V. L., 2014, "Alloy Negative Electrodes for Li-Ion Batteries," *Chem. Rev.*, **114**(23), pp. 11444–11502.
- [155] Whittingham, M. S., 2004, "Lithium Batteries and Cathode Materials," *Chem. Rev.*, **104**(10), pp. 4271–4302.
- [156] Bruce, P. G., Scrosati, B., and Tarascon, J. M., 2008, "Nanomaterials for Rechargeable Lithium Batteries," *Angew. Chem. Int. Ed.*, **47**(16), pp. 2930–2946.
- [157] Liu, G., Zheng, H., Kim, S., Deng, Y., Minor, A. M., Song, X., and Battaglia, V. S., 2008, "Effects of Various Conductive Additive and Polymeric Binder Contents on the Performance of a Lithium-Ion Composite Cathode," *J. Electrochem. Soc.*, **155**(12), pp. A887–A892.
- [158] Xu, R., and Zhao, K., 2016, "Electrochemomechanics of Electrodes in Li-Ion Batteries: A Review," *ASME J. Electrochem. Energy Convers. Storage*, **13**(3), p. 030803.
- [159] Smith, K. C., Mukherjee, P. P., and Fisher, T. S., 2012, "Columnar Order in Jammed LiFePO₄ Cathodes: Ion Transport Catastrophe and Its Mitigation," *Phys. Chem. Chem. Phys.*, **14**(19), pp. 7040–7050.
- [160] Saravanan, K., Balaya, P., Reddy, M. V., Chowdari, B. V. R., and Vittal, J. J., 2010, "Morphology Controlled Synthesis of LiFePO₄/C Nanoplates for Li-Ion Batteries," *Energy Environ. Sci.*, **3**(4), pp. 457–463.
- [161] Cho, S., Chen, C. F., and Mukherjee, P. P., 2015, "Influence of Microstructure on Impedance Response in Intercalation Electrodes," *J. Electrochem. Soc.*, **162**(7), pp. A1202–A1214.
- [162] Chen, C. F., Barai, P., and Mukherjee, P. P., 2014, "Diffusion Induced Damage and Impedance Response in Lithium-Ion Battery Electrodes," *J. Electrochem. Soc.*, **161**(14), pp. A2138–A2152.
- [163] Chen, C. F., Barai, P., and Mukherjee, P. P., 2016, "An Overview of Degradation Phenomena Modeling in Lithium-Ion Battery Electrodes," *Curr. Opin. Chem. Eng.*, **13**, pp. 82–90.
- [164] Chen, C. F., and Mukherjee, P. P., 2015, "Probing the Morphological Influence on Solid Electrolyte Interphase and Impedance Response in Intercalation Electrodes," *Phys. Chem. Chem. Phys.*, **17**(15), pp. 9812–9827.